AWARD NUMBER: W81XWH-13-1-0467

TITLE: Preventing Prostate Cancer Metastasis by Targeting Exosome Secretion

PRINCIPAL INVESTIGATOR: Christine Vogel

CONTRACTING ORGANIZATION: New York University

New York, NY 10012-2331

REPORT DATE: December 2015

TYPE OF REPORT: Final

PREPARED FOR: U.S. Army Medical Research and Materiel Command
Fort Detrick, Maryland 21702-5012

DISTRIBUTION STATEMENT: Approved for Public Release;
Distribution Unlimited

The views, opinions and/or findings contained in this report are those of the author(s) and should not be construed as an official Department of the Army position, policy or decision unless so designated by other documentation.

REPORT DOCUMENTATION PAGE

Form Approved
OMB No. 0704-0188

1. REPORT DATE	2. REPORT TYPE	3. DATES COVERED
December 2015	Final	30Sep2013 - 29Sep2015

4. TITLE AND SUBTITLE

Preventing Prostate Cancer Metastasis by Targeting Exosome Secretion

5a. CONTRACT NUMBER
W81XWH-13-1-0467 MOD P00001

5b. GRANT NUMBER
A13-0384-002; F4763

5c. PROGRAM ELEMENT NUMBER

6. AUTHOR(S)

Christine Vogel

E-Mail: cvogel@nyu.edu

5d. PROJECT NUMBER

5e. TASK NUMBER

5f. WORK UNIT NUMBER

7. PERFORMING ORGANIZATION NAME(S) AND ADDRESS(ES)

New York University
New York 10003 NY

8. PERFORMING ORGANIZATION REPORT NUMBER

9. SPONSORING / MONITORING AGENCY NAME(S) AND ADDRESS(ES)

U.S. Army Medical Research and Materiel Command

Fort Detrick, Maryland 21702-5012

10. SPONSOR/MONITOR'S ACRONYM(S)

11. SPONSOR/MONITOR'S REPORT NUMBER(S)

12. DISTRIBUTION / AVAILABILITY STATEMENT

Approved for Public Release; Distribution Unlimited

13. SUPPLEMENTARY NOTES

14. ABSTRACT

We hypothesized that exosomes secreted by advanced prostate cancer cells groom stromal cells at pre-metastatic sites to render the bone microenvironment more favorable for metastatic growth. Testing this hypothesis has direct relevance towards an understanding of the often lethal complications of prostate cancer, manifested in extensive and painful metastasis of the bone. We proposed compare the impact of exosomes derived from advanced stage prostate cancer on bone stromal cells by extracting vesicles from medium conditioned by metastatic and non-metastatic prostate cancer cells. We successfully established sensitive cancer proteomics analyses in our lab. We optimized the growth conditions and experimental parameters to test exosome secretion and effects in prostate cancer cells and bone marrow cells. We found that the cell lines in contrast to tissue samples) do not secrete enough exosomes for efficient quantitative analysis, as was verified by a number of orthogonal approaches.

15. SUBJECT TERMS

Exosomes; cancer proteomics; ultracentrifugation; secretome; prostate cancer; metastasis

16. SECURITY CLASSIFICATION OF:			17. LIMITATION OF ABSTRACT	18. Page numbers	19a. NAME OF RESPONSIBLE PERSON
a. REPORT	b. ABSTRACT	c. THIS PAGE			USAMRMC
Unclassified	Unclassified	Unclassified	UU	63	19b. TELEPHONE NUMBER *(include area code)*

Standard Form 298 (Rev. 8-98)
Prescribed by ANSI Std. Z39.18

Table of Contents

Table of Contents 3
Revised version 4
Response to reviewer's criticisms 4
1. INTRODUCTION 5
2. KEYWORDS 5
3. ACCOMLISHMENTS 6
What were the major goals of the project? 6
What was accomplished under these goals? 6
What opportunities for training and professional development has the project provided? 14
How were the results disseminated to communities of interest? 14
What do you plan to do during the next reporting period to accomplish the goals? 14
4. IMPACT 15
What was the impact on the development of the principal discipline(s) of the project? 15
What was the impact on other disciplines? 15
What was the impact on technology transfer? 15
What was the impact on society beyond science and technology? 15
5. CHANGES/PROBLEMS: 15
6. PRODUCTS 16
4. PARTICIPANTS & OTHER COLLABORATING ORGANIZATIONS 16
What individuals have worked on the project? 16
Has there been a change in the active other support of the PD/PI(s) or senior/key personnel since the last reporting period? 17
What other organizations were involved as partners? 17
5. APPENDICES 17
A. References 17
B. Christine Vogel (PI) – Curriculum Vitae 18
C. Product (published) 21
D. Manuscript (in preparation) 22

Revised version

Highlighted in BLUE are changes compared to the previous version of the report.

Response to reviewer's criticisms

The PI's responses are printed in bold letters.

Reviewer's Comments:
- The data presentation in the body of the report is not comprehensive for all reported results. Data from the appended draft manuscript are not directly cited in the body of the report to support key research findings. A revised report is needed.

We included additional figures and tables to support the results.

We also incorporated a reference to the draft manuscript in the text. We explain below how the personnel changes resulted in inclusion of these manuscripts in products acknowledged for DOD funding.

The main tasks of this project are not completed and there is no indication that the PI has filed for a second no cost extension.

This Hypothesis Testing grant provided a budget of $75,000. The highly challenging work required advanced research personnel, which resulted in a post-doctoral researcher, Dr. Rebecca Bish working on the project (4 months). The researcher left the lab and project early for private reasons.

After the PI Vogel returned from medical leave (brain tumor), she employed a part-time student worker (Dionne Argyle, 8 months, 10 hrs/week) and one of the graduate students (Zhe Cheng, 5.5 months). Again, challenges in the experimental procedures prevented much progress by the time the grant's funds were exhausted.

Therefore, Vogel asked another post-doctoral researcher, Dr. Nerea Cuevas-Polo, to work part-time on the project during the first no-cost extension period. Dr. Cuevas-Polo worked on the project for six months, but was paid from a different funding source.

Dr. Cuevas-Polo (based on the work achieved in the first reporting period) established the protocol to extract exosomes using ultra-centrifugation and, together with Dionne Argyle, conducted the medium-transfer experiments (see below). Both the extraction method and the medium transfer experiments were essential parts of the project, but took a long time to perform as explained below. Therefore, once Dr. Cuevas-Polo's contract finished, the project had to be closed due to lack of personnel and funds without having been able to achieve the final goals.

Task 2, Subtask 1 was reported to be in progress during the first reporting period. No update is given in this final report. The report should be revised to include all work performed during the entire award period.

Task 2, Subtask 1 concerned the response of bone marrow cells to treatment with exosomes secreted from metastatic vs. non-metastatic prostate cancer cells. In the last report, we proposed to test first

the response to transfer of medium conditioned by prostate cancer cells. The revised report includes results from these tests.

CDMRP Technical Reporting Requirements state that the report should include "pertinent data and graphs in sufficient detail to explain any significant results achieved." The PI should revise the report to include all relevant data.

The revised report including additional figures, tables, and text, is attached below.

1. INTRODUCTION

Bone metastasis is a painful and often lethal complication of prostate cancer. For the proposed project, we hypothesized that exosomes secreted by advanced prostate cancer cells groom stromal cells at pre-metastatic sites to render the bone microenvironment more favorable for metastatic growth. We generated this hypothesis by using a probabilistic gene functional network to re-analyze a publicly available dataset in which transcript levels of androgen-responsive genes are compared between early- and advanced/metastatic prostate cancer [1]. The hypothesis was also supported by recent findings in exosomes secreted by melanoma cells [2]. We proposed to test the hypothesis by examining the effects and contents of exosomes derived from advanced stage prostate cancer. **Aim 1** proposed a quantitative comparison of changes in the structure and cargo of exosomes derived from early versus advanced prostate cancer cell lines to identify mechanisms of action (using large-scale, high-resolution proteomics). **Aim 2** proposed to profile alterations in potential target stromal cells upon exposure to early versus late prostate cancer exosomes to determine the effect on the metastatic microenvironment (using next-generation sequencing and proteomics). To perform these analyses, we i) successfully established the pipelines needed for sensitive cancer proteomics in the lab; ii) successfully established the prostate cancer and bone marrow cells lines in the lab; iii) successfully extracted exosomes from the media, using a variety of approaches; and iv) established that currently achieved quantities of exosomes were insufficient for the proposed analyses and a new cell model as to be identified.

Excerpt from previous report on project progress and changes:

Re Task 1: Polymer removal from mass spectrometry samples. "We also conducted preliminary mass spectrometry studies with the isolated exosomes. However, we identified only few proteins due to sample contamination with polymers that originated from the isolation kits. We are working with the companies to address these issues, i.e. remove the polymers prior to mass spectrometry analysis. Encouragingly, our preliminary proteomics analysis of prostate exosome samples identified several typical exosome markers, as defined by Exocarta (http://www.exocarta.org/exosome_markers)."

Re Task 2: Testing of pre-conditioned media on bone marrow cells. "Due to the difficulties with the commercially available exosome isolation kits, we explored alternative ways to test the proposal's hypothesis. One route includes a pilot study in which we use the *secretome*, i.e. the entirety of the secreted protein samples, including exosomes and other extracellular vesicles, to treat bone marrow cells. We will then test the cells for commonly used markers of bone metastasis or a pre-metastatic state, i.e. MET from ref. [2], α-6 and α-2 integrin, ALP and endothelin-1. "

2. KEYWORDS

Exosomes; cancer proteomics; ultracentrifugation; secretome; prostate cancer; metastasis

3. ACCOMLISHMENTS

What were the major goals of the project?

Goal 1:
Establish sensitive cancer proteomics using mass spectrometry

Goal 2:
Establish growth of prostate cancer and bone marrow cell lines in the lab

Goal 3:
Optimize experimental conditions for exosome extraction and transfer

Goal 4:
Quantitative comparison of changes in the structure and cargo of exosomes derived from early versus advanced prostate cancer cell lines to identify mechanisms of action (using large-scale, high-resolution proteomics) (Aim 1 / Task 1)

Goal 5:
Profile alterations in potential target stromal cells upon exposure to early versus late prostate cancer exosomes to determine the effect on the metastatic microenvironment (using next-generation sequencing and proteomics) (Aim 2 / Task 2)

What was accomplished under these goals?

Goal 1: Establish sensitive cancer proteomics using mass spectrometry

Our laboratory uses mass spectrometry to quantify protein concentrations. In this goal, personnel from this grant (Bish, Cuevas-Polo, Cheng, Vogel) worked on establishing these proteomics methods within the cancer system. Establishing these methods involved optimization of sample preparation, optimization of mass spectrometry runs, and statistical data analysis. We successfully established this pipeline in two proteomics projects – one of which has led to a published paper, the other one has a paper manuscript in preparation.

1. Bish R, Cuevas-Polo N, Cheng Z, Hambardzumyan D, Munschauer M, Landthaler M, Vogel C. Comprehensive Protein Interactome Analysis of a Key RNA Helicase: Detection of Novel Stress Granule Proteins. Biomolecules. 2015 Jul 15;5(3):1441-66. doi: 10.3390/biom5031441. http://www.ncbi.nlm.nih.gov/pubmed/26184334
2. Cuevas-Polo N, Vo D, Qiao M, Choi H, Anant S, Penalva LO, Vogel C. Integrative proteomics analysis of the relationship between the RNA-binding Musashi 1 and miR124. *Under preparation*

Both publications / manuscript drafts are related to this report in two ways.

1) The project in this proposal requires expert use of quantitative, high-resolution proteomics to monitor changes in cancer cell proteomes. The two projects whose publication/manuscript are listed above, served to establish the necessary quantitative methods and to train personnel involved in the work in the proteomic workflow that is used in the Vogel lab.

2) Key personnel from this grant, such as Dr. Rebecca Bish and Dr. Nerea Cuevas-Polo, and the graduate students Dionne Argyle and Zhe Cheng were part of the above projects.

The PI received 0.25 summer months payment (1 year) from this grant, and therefore acknowledges DOD funding in another publication which appeared after the first version of this report was submitted. The publication is an invited interview / perspective article with the PI in the open access journal *PLoS Computational Biology*.

3. Vogel C. Systems Approaches to the Eukaryotic Stress Response. PLoS Comp Biology. 2016 Mar 10;12(3):e1004757. doi: 10.1371/journal.pcbi.1004757. http://www.ncbi.nlm.nih.gov/pubmed/26963258

Goal 2: Establish growth of prostate cancer and bone marrow cell lines in the lab

We established growth protocols for two prostate cancer cell lines LnCAP (non-metastatic) and LNCaP C4-2b (metastatic). To avoid contamination by exosomes from the fetal bovine serum (FBS) supplement that is part of mammalian cell growth media, we tested if the cells grow in FBS-free medium. As the cells did not grow well (*not shown*), we tested an alternative method in which cells were grown in medium with exosome-depleted FBS (commercially available). Cells grew well with normal phenotype (*not shown*). We also established growth of two bone marrow cell lines (HS-27A and hFOB1.19) in normal medium supplemented with FBS-free medium. Again, the cells showed normal phenotypes (*not shown*). However, as explained in **Goal 3**, we faced additional challenges using these growth conditions.

Goal 3: Optimize experimental conditions for exosome extraction and transfer

And

Goals 4: Quantitative comparison of changes in the structure and cargo of exosomes derived from early versus advanced prostate cancer cell lines to identify mechanisms of action (using large-scale, high-resolution proteomics) (Aim 1 / Task 1).

While several approaches exist to extract exosomes from body fluids for biomarker screenings, several additional challenges exist when working with cell lines: 1) cell growth conditions have to avoid contamination by exosomes present in the unconditioned medium; 2) exosomes have to be secreted in quantities sufficient for proteomics analysis; and 3) exosome isolation protocols cannot include detergents in the final mass spectrometry samples. We have worked towards overcoming these challenges.

FBS contains plenty of bovine exosomes which have to be removed prior to culturing human cells in the medium. As explained in **Goal 2**, we therefore tested FBS-free medium and medium with exosome-depleted FBS. As the cells had normal phenotypes and growth rates in the latter, we decided to proceed with exosome-depleted FBS which was commercially available.

Next, we tested a variety of commercially available exosome-isolation kits (**Table 1**) in their ability to isolate exosomes that were a) positive with respect to exosome markers, and b) provided enough material for proteomics analysis.

Table 1. Exosome isolation kits tested

Name of the kit used	Amount of Starting Material	Preparation/ Methods	Preparation Time	End Sample Amount
ExoQuick by System Biosciences	10mL of Cell Culture Media + 2 mL of ExoQuick-TC Exosome Precipitation Solution	Centrifugation (removal of cell debris) Overnight incubation (4 degrees) Centrifugation	- Day 1: 20- 30 minutes - Day 2: 45-60 minutes	100-500uL
Total Exosome	10mL of Cell Culture Media +	Centrifugation (removal of cell debris)	- Day 1: 45-60	100uL

Isolation Reagent by Invitrogen	5mL of Total Exosome Isolation Reagent	Overnight incubation (4 degrees with rotation) Ultracentifugation	minutes - Day 2: 75-90 minutes	
Pure Exo by 101 Bio	4mL of Cell Culture Media+ 1mL (Solutions A+B+C)	Centrifugation (removal of cell debris) Vorxtexing 4 degree incubation Column separation/purification	- 1-2 hours	50-200uL
ExoSpin by Cell Guidance Systems	6mL of Cell Culture Media + Buffer A (2mL)	Centrifugation (removal of cell debris) Overnight incubation (4 degrees with rotation) Ultracentrifugation Column purification	- Day 1: 45-60 minutes - Day 2: 2 hours	200uL

As **Figure 1** shows, the different kits provided different quantities of protein after exosome isolation. Only samples with clearly visible staining on a Coomassie gel are suitable for mass spectrometry analysis. **Figure 1** shows that the Invitrogen, ExoQuick, and ExoSpin kits provide protein samples covering a wide range of molecular weights.

To validate the specificity of exosome isolation of the four kits, we used established exosome markers (CD9, CD81, Hsp70) in western blot experiments (**Figure 2**). The ExoQuick and ExoSpin kits are positive for all three markers without extensive unspecific bands (**Figure 2**); the ExoSpin kit (Cell Guidance) provides the most consistent results combined with quantitative protein extraction over a large range of molecular weights (see item 2, **Figure 1**). Therefore, we used this kit for subsequent protocol optimization.

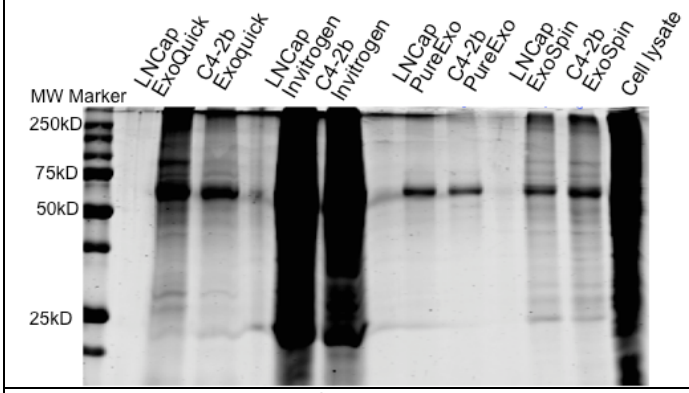

Figure 1. Protein gels for exosomal samples isolated with different kits (Table 1). Staining is for all proteins (Coomassie)

To perform mass spectrometry experiments, a minimum protein amount of 20 ug is required. Since exosomes are small vesicles secreted from the cells, they are highly diluted in the growth medium. Our optimization resulted in use of 20 ml of conditioned medium (2 days growth in medium with exosome-depleted FBS) to extract enough sample with the ExoSpin kit.

When conducting mass spectrometry experiments with the samples isolated using the ExoSpin kit, protein identification was very low (<80 proteins) and the peptide chromatographic image was severely affected. These findings suggested detergent or polymer in the sample. It is essential for high-resolution mass spectrometry to remove *any* polymer and detergent prior to analysis, as these molecules are extremely harmful for the liquid chromatography step on a reverse phase column. Severe detergent contamination results in loss of the column (at least $500 each).

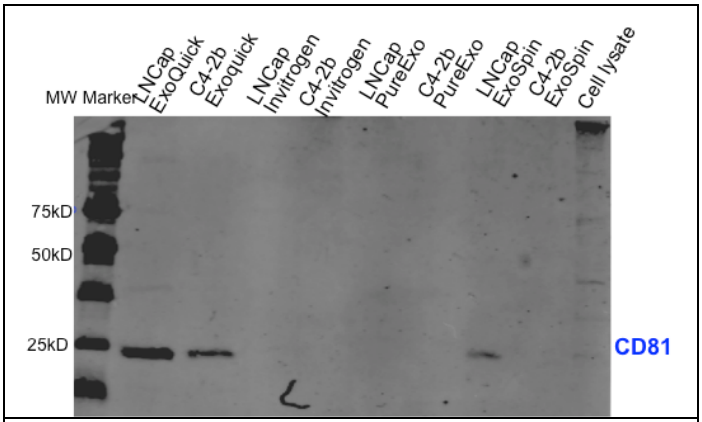

Figure 2. Western blots with antibodies against four exosome markers. Only CD81 showed a signal.

Our next efforts were therefore two-fold: a) identify the source of the detergent, and b) identify efficient methods to remove the detergent while retaining enough proteomic sample for mass spectrometry analysis.

At first we suspected the detergent to originate from the ExoSpin exosome isolation kit which was confirmed by the supplier. We tested different detergent removal methods:

- Use of a detergent removal kit (OrgoSol, G-Biosciences) which resulted in so much sample loss that proteomics analysis was infeasible.
- Filtering once using filters provided by Cell Guidance, the company that produced the ExoSpin exosome isolation kit, as recommended by the suppliers. Due to sample loss, we again scaled up the number of cells used for one sample. However, when examining the sample by mass spectrometry, we again detected detergent. We identified 35 proteins, most of them high-abundance proteins without links to exosomes, i.e. they were not reported in ExoCarta (http://www.exocarta.org/exosome_markers).
- Filtering twice with Cell Guidance filters. However, when examining the sample by mass spectrometry, we again detected detergent. We identified 42 proteins, again, without connection to exosomes.

These results were unexpected as we had strictly followed company instructions. With each detergent-contaminated mass spectrometry run we lost the chromatographic column. Therefore, we had to put proteomics experiment on halt until the source of detergent was identified.

First, we tested alternative methods for exosome isolation that did not involve commercially available kits, i.e. repeated ultra-centrifugation (UC), according to established protocols [4]. The protocol consisted of consecutive steps of UC at different speeds and isolation of specific fractions enriched for the desired organelle. This method is considered the gold-standard of exosome isolation and very robust.None of the buffers involved contains any detergent. Indeed, this method led to isolation of high-quality exosomes that tested positive for the respective markers (**Figure 3**).

We used 30 ml medium (with exosome-depleted FBS) conditioned by prostate cancer cells for two days. However, when analyzing the UC-based exosome samples via mass spectrometry, we unexpectedly detected detergent in the sample again.

We proceeded to test all components of the entire workflow and eventually found that exosome-depleted FBS contains detergent at high levels which then contaminated all samples, even after repeated use of detergent-removal filters (see above).

Therefore, we investigated alternative methods to deplete FBS of bovine exosomes, not using the commercially available exosome-depleted FBS. After several rounds of optimization, we established a protocol in which FBS was depleted of bovine exosomes using dual ultra-centrifugation. We also revisited the earlier attempts to grow cells in FBS-free medium (**Figure 3**).

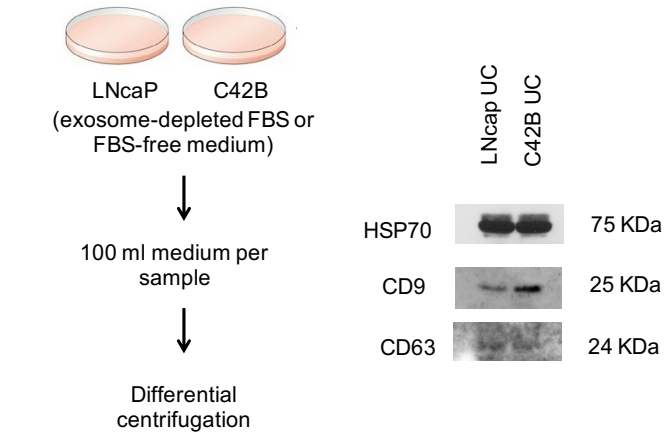

Figure 3. Final protocol and results for exosome isolation from condition medium.

The final, optimized protocol for cell line growth and exosome isolation involved use of UC-based exosome-depleted FBS in the growth medium and UC-based isolation of exosomes (**Figure 3**). With this protocol, we obtained high-quality exosomes from the conditioned medium. The samples did not contain detergent and were therefore suited for mass spectrometry analysis. Using at least 100 ml of conditioned medium provided enough sample for one mass spectrometry run (without extensive sample fractionation).

However, the ultra-centrifuge available at NYU Biology only carried rotors that allowed for a maximum of 6 tubes with 50 ml volume. Due to this limitation and because of the extensive UC use required by the protocol, we could only process three samples at a time. Issues like these caused the very slow progress with the project.

We contacted Dr. Lara Mahal from NYU Chemistry who successfully isolates exosomes from melanoma cell lines. Mahal confirmed that different cell lines secrete very different amounts of exosomes, and that some cell lines secreted so few exosomes that their quantitative isolation is practically infeasible. She also recommended use of at least 100 ml of medium.

The melanoma cell line used in reference publication [2] and used by Mahal produce a large amont of exosomes – however, the prostate cancer cell lines tested in our case produce comparatively few. This challenge can be addressed by i) scaling up the protocols, or ii) testing different prostate cancer cell lines if they secrete more exosomes.

Goal 3: Optimize experimental conditions for exosome extraction and transfer

And

Goal 5: Profile alterations in potential target stromal cells upon exposure to early versus late prostate cancer exosomes to determine the effect on the metastatic microenvironment (using next-generation sequencing and proteomics) (Aim 2 / Task 2)

While working on the above steps to isolate exosomes for proteomics analysis and the proposed transfer experiments, we also worked on optimizing the conditions at which bone marrow cells should be incubated with exosomes/microvesicles. The original experiment proposed transfer of exosomes isolated from medium conditioned by metastatic and non-metastatic prostate cancer cells to medium of bone marrow cells, and monitoring changes in bone marrow cells towards the pre-metastatic niche. This experiment represents the central hypothesis of this grant.

However, due to the problems with exosome isolation (see above), we started out by conducting experiments in which (instead of isolated exosomes) we transferred the entire pre-conditioned medium between cell cultures to test its effect on formation of the pre-metastatic niche state in bone marrow cells and osteoblasts. This medium-transfer experiment is outlined in **Figure 4.**

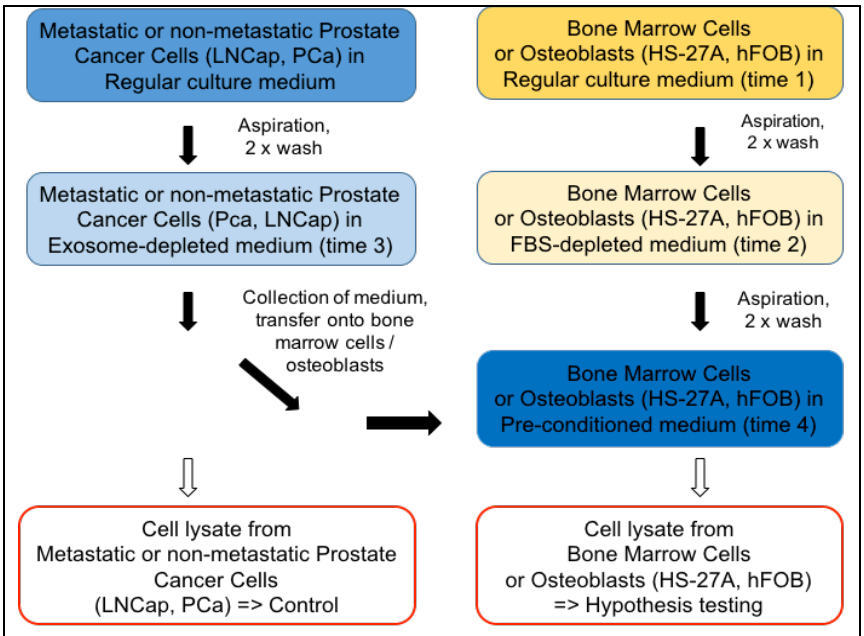

Figure 4. Outline for medium transfer experiment

The experiment has several steps that needed to be optimized. Incubation time periods 1 to 4 (**Figure 4**) were tested in a range between 12 to 72 hours. Time 1 describes the normal growth of bone marrow cells/osteoblasts, i.e. time between two passages or one passage and the next step of the experiment. Time 2 describes a 'starvation' step in which the cells are primed towards uptake of exosomes by growing them in medium that contains exosome-depleted FBS. Twenty-four hours of this 'starvation' period proved to be sufficient. Time 3 describes the time needed to condition the medium with metastatic or non-metastatic prostate cancer cells. While 72 hours produced the highest concentration of exosome in the growth medium, it also led to depletion of the medium with nutrients, rendering it less useful for transfer and incubation with bone marrow cells. Time 4 describes the time bone marrow

cells / osteoblasts grow in the conditioned medium. This period is also crucial as expected changes in cells might only occur after days of incubation which again is not feasible if the growth medium becomes depleted in nutrients.

Therefore, we optimized the medium transfer experiment to accumulate maximal amounts of exosomes in the medium and minimize depletion of nutrients.

In addition, to test for a response in bone marrow cells / osteoblasts, we employed western blotting to test for putative markers of formation of the pre-metastatic niche (according to the proposal's central hypothesis). As the pre-metastatic niche is less well-defined that metastasis, we first conducted a thorough literature search to identify a number of candidate markers. These putative markers are summarized in **Table 2**.

Table 2. Possible Markers for Metastasis in Osteoblasts/Prostate Cancer
This table lists a number of potential candidates that can be evidence for the establishment of the pre-metastatic niche, readying tumor cells for metastasis. Name and function of the candidates are the first two columns. Possible antibodies for testing and references providing evidence are listed in the last two columns.

Possible Marker	Relationship to formation of pre-metastatic niche	Antibodies	Reference
Endothelin-1	Implicated in osteoblastic metastasis from breast cancer.	Anti-Endothelin 1 antibody (ab88093) ET-1 antibody (N-8) sc-21625	Guise, Theresa A., Juan Juan Yin, and Khalid S. Mohammad. "Role of endothelin-1 in osteoblastic bone metastases." *Cancer* 97.S3 (2003): 779-784.
c-kit	Loss of BRCA2 function stimulates prostate cancer (PCa) cell invasion and is associated with more aggressive and metastatic tumors in PCa patients. Concurrently, the receptor tyrosine kinase c-kit is highly expressed in skeletal metastases of PCa patients and induced in PCa cells placed into the bone microenvironment in experimental models.	c-Kit (phosphor Tyr730) antibody (GTX25633) Anti-ckit antibody (ab5506)	Mainetti, Leandro E., et al. "Bone-induced c-kit expression in prostate cancer: A driver of intraosseous tumor growth." *International Journal of Cancer* (2014).
VEGF	"bone-marrow derived haematopietic progenitor cells that express VEGF1 home to tumor-specific pre-metastatic sites and form cellular clusters before the arrival of tumor cells."	Anti-VEGFA antibody (ab183100) Anti-VEGFA antibody (ab51745)	Kaplan, Rosandra N., et al. "VEGFR1-positive haematopoietic bone marrow progenitors initiate the pre-metastatic niche." *Nature* 438.7069 (2005): 820-827.
BMP-6	BMP-6 was the only protein that was not expressed in the non-metastatic group but was in 55% of patients with established skeletal metastases.	BMP6 antibody [morph-6.1] ab15640	Thomas, B. G., and F. C. Hamdy. "Bone morphogenetic protein-6: potential mediator of osteoblastic metastases in prostate cancer." *Prostate cancer and prostatic diseases* 3.4 (2000): 283-285.
LOX	LOX-mediated pre-metastatic focal osteolytic lesions generate niches within the bone microenvironment that support colonization of circulating tumor cells and the formation of overt metastases.	LOX antibody (NB100-2527) LOX (F-8) sc-373995	Cox, Thomas R., et al. "The hypoxic cancer secretome induces pre-metastatic bone lesions through lysyl oxidase." *Nature* (2015).
MMP-9	"In addition osteoblast-conditioned medium was found to stimulate prostate cancer cells into producing MMP-9 and uPA, while at the same time increasing the rate of prostate cancer proliferation."	MMP-9 antibody (3852S) MMP-9 (2C3) sc-21733 MMP-9 (4A3)	Ibrahim, Toni, et al. "Pathogenesis of osteoblastic bone metastases from prostate cancer." *Cancer* 116.6 (2010): 1406-1418.
MMP-2	"MMP2 and MMP 9 are both induced in the pre-metastatic niche and hypoxic regions and moreover been shown to promote activation of latent TGF-beta by cleaving the mature cytokine leading to cancer invasion and angiogenesis in mammary carcinoma models."	MMP-2 antibody (4022S) Anti-MMP-2 antibody (ab37150)	Descot, Arnaud, and Thordur Oskarsson. "The molecular composition of the metastatic niche." *Experimental cell research* 319.11 (2013): 1679-1686.
Carcinoembryonic antigen	"with surprisingly diverse functions in cell adhesion, in intracellular and intercellular signaling, and during complex biological processes such as cancer progression, inflammation, angiogenesis, and metastasis"	Monoclonal Anti-CEA antibody C2331	Gerhard, Markus, et al. "Specific detection of carcinoembryonic antigen-expressing tumor cells in bone marrow aspirates by polymerase chain reaction."*Journal of clinical oncology* 12.4 (1994): 725-729.
BMP-7	Bone morphogenetic proteins (BMPs) have been implicated in tumorigenesis and metastatic progression in various types of cancer cells.	Anti-BMP7 (ab56023) BMP-7 antibody (L-19) sc-9305	Morrissey, Colm, et al. "Bone morphogenetic protein 7 is expressed in prostate cancer metastases and its effects on prostate tumor cells depend on cell phenotype and the tumor microenvironment." *Neoplasia* 12.2 (2010):

			192-205.
PDGF-D	Both PDGF receptor β (β-PDGFR) and its ligand PDGF D are up-regulated in primary prostate cancers and bone metastases.	PDGF-D (R-20) sc-23573	Conley-LaComb, M. Katie, et al. "PTEN regulates PDGF ligand switch for β-PDGFR signaling in prostate cancer." *The American journal of pathology* 180.3 (2012): 1017-1027.
Osteoprotegerin	Osteoprotegerin (OPG), a critical regulator of osteoclastogenesis, is expressed by prostate cancer cells, and OPG levels are increased in patients with prostate cancer bone metastases.	Anti- OPG antibody (ab9986) OPG antibody (EPR3592)	Corey, Eva, et al. "Osteoprotegerin in prostate cancer bone metastasis."*Cancer research* 65.5 (2005): 1710-1718.
VCAM-1	Inhibiting signaling between vascular cell adhesion molecule-1 and its receptor, integrin α4, prevents bone metastases in mouse models of breast cancer.	VCAM-1 antibody (12367S) VCAM-1 (H-276) sc-8304	Haas, Michael J. "VCAM-1 engine drives bone metastases." *SciBX: Science-Business eXchange* 5.2 (2012).
Fibronectin	"Fibronectin deposition appears to be a critical factor regulating the pre-metastatic niche formation and fibronectin matrices have been found to provide specific microenvironments to regulate LOX catalytic activity."	Anti-Fibronectin antibody (ab299) Anti-Fibronectin antibody (ab25583)	Peinado, Héctor, Simon Lavotshkin, and David Lyden. "The secreted factors responsible for pre-metastatic niche formation: old sayings and new thoughts."*Seminars in cancer biology*. Vol. 21. No. 2. Academic Press, 2011.

From **Table 2**, we selected markers of pre-metastatic niche formation and tested them in western blots of cell lysate from bone marrow cells / osteoblasts (HS-27A, hFOB1.19) and incubated for different times with medium pre-conditioned by metastatic and non-metastatic prostate cancer cells (C4-2b, LNCap), respectively. Time 4 (**Figure 4**) was varied between 24, 48, and 72 hours. **Figure 5** shows the results of the medium-transfer experiments. Due to a switch in providers of membranes for western blots, some of the blots are less than optimal and would need to be repeated.

Despite some unspecific bands, **Figure 5** shows clear bands at the correct molecular weight for several of the selected proteins. The clearest signal arises from LOX which is not found in untreated bone marrow cells / osteoblasts, but found after incubation with pre-conditioned medium, both in the mature and the glycosylated form. However, LOX occurs in both samples incubated with 'metastatic' and 'non-metastatic' medium. In the lanes at the far right of the western blots in which the osteoblasts are treated with medium from non-metastatic LnCap and metastatic C4-2b cells, prespectively, we observe more mature LOX in the cells treated with medium conditioned by metastatic prostate cancer cells. This difference is not seen for the bone marrow cells, and might indicate a true signal that distinguishes the two different media in their effect on osteblasts. This observation will need to be confirmed in replicate experiments.

A similar signal can be seen for C-kit which displays a difference for the treated osteobloasts, but not the bone marrow cells. In the osteoblasts, we observe a stronger response for the cells treated with 'metastatic' medium for either 48 or 72 hours than for the cells treated with 'non-metastatic' medium. Again, due to the abundance of unspecific bands, this result will have to be reproduced in a replicate experiment.

BMP-6 and MMP-9 are also clearly identifiable, but are indifferent to the type of treatment. The western blot for VEGFR suggests a time-dependence of the response, in particular in the osteoblasts, with 48 hours providing a stronger signal than 24 hours incubation.

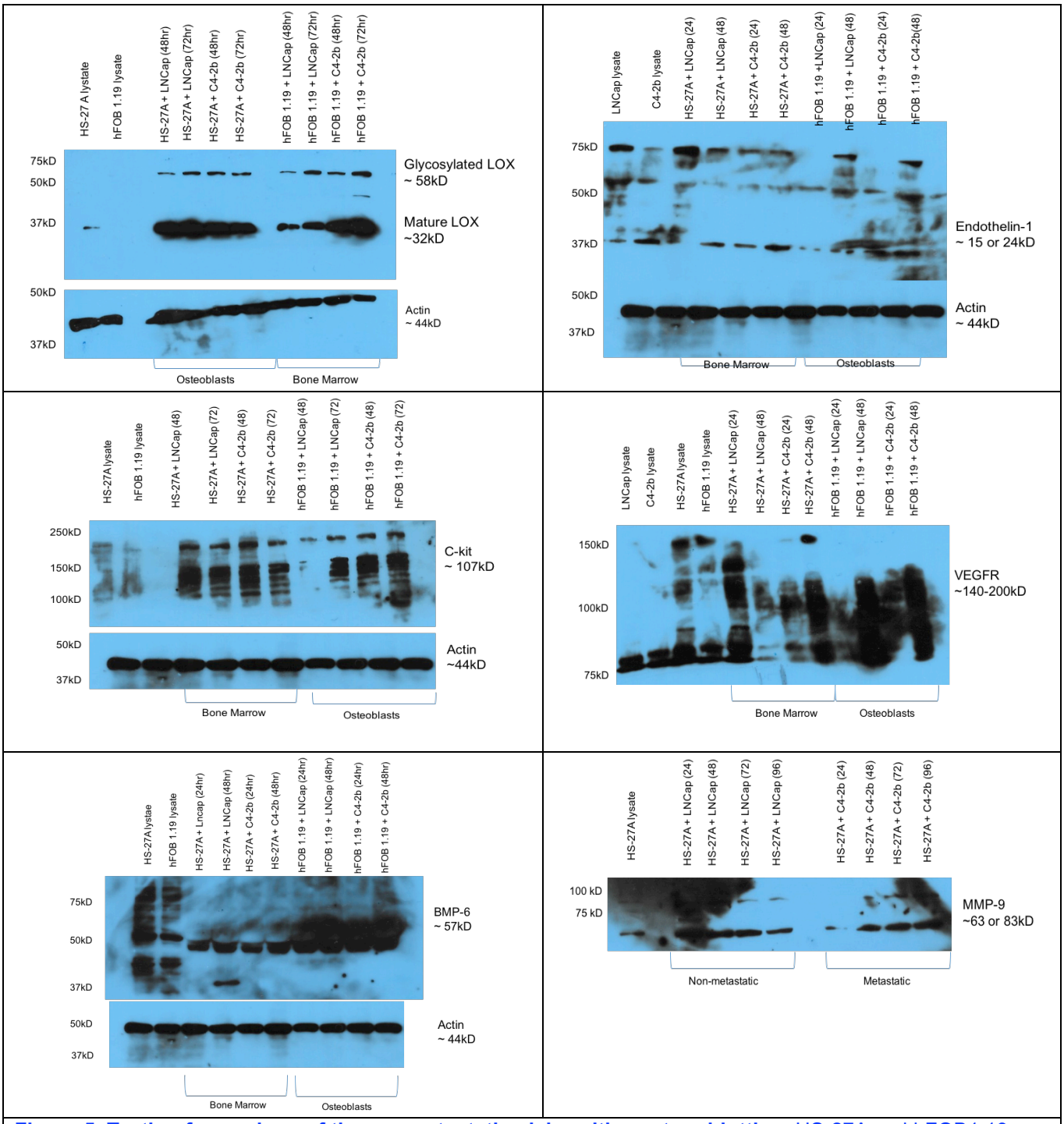

Figure 5. Testing for markers of the pre-metastatic niche with western blotting. HS-27A and hFOB1.19 are the bone marrow cells and osteoblasts used, respectively. The time periods in brackets refer to incubation with pre-conditioned medium (time 4, **Figure 4**). LNCap and C4-2b are the non-metastatic and metastatic prostate cancer cell lines, respectively, that were used to condition the medium for 24hours (time 3, **Figure 4**). From top left to bottom left, the following putative markers were tested: LOX, Endothelin-1, C-kit, VEGFR, BMP-6, and MMP9.

We then repeated some of the western blots with slightly altered conditions (**Figure 6**). We observed no difference in the response for Endothelin-1. For c-it, the response in the osteoblasts (hFOB) treated with medium conditioned by metastatic prostate cancer cells C2-4B (C24B) is slightly stronger than in the non-metastic (LNCap) and bone marrow (HS27) control, but the difference is not strong enough for clear conclusions. The small difference might be due to the fact that the incubation time (time 4, **Figure 4**) only lasted for six hours.

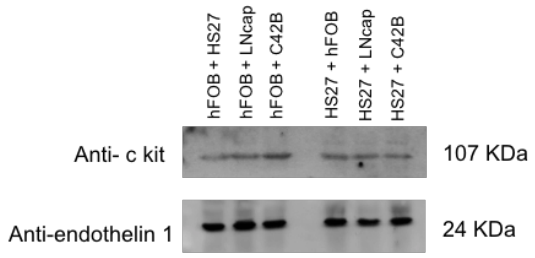

Figure 6. Testing for markers of the pre-metastatic niche with western blotting. HS-27A and hFOB1.19 are the bone marrow cells and osteoblasts used, respectively. LNCap and C4-2b are the non-metastatic and metastatic prostate cancer cell lines that were used to condition the medium. Cells were starved for 24 hours (time 2, see **Figure 4**), incubated for six hours with medium (time 4) which had been conditioned for 48 hours (time 3).

In sum: the results from **Figures 5 and 6** suggest first putative markers for formation of the pre-metastatic niche in osteoblasts based on treatment with medium conditioned with metastatic prostate cancer cells. The results also suggest conditions under which this effect is maximal. However, all western blots need to be repeated at higher quality. Future experiments should confirm the differential response in LOX and C-kit expression levels in osteoblasts. Further, fine-tuning of the time-dependent VEGFR response might provide another marker testable for differences between the effects of medium from metastatic vs. non-metastatic prostate cancer cells. The results from these experiments suggest the use of a conditioning and incubation time of 24 and 48 hours, respectively (times 3 and 4, **Figure 4**). Pre-starving of osteoblasts and bone marrow cells for 24 hours (time 2) is beneficial for the results. While based on the current results it is too early to draw firm conclusions on the acceptance or rejection of the major hypothesis tested in this grant, current results are consistent with the fact that molecules secreted by metastatic prostate cancer cells might transform osteoblasts towards the pre-metastatic niche.

What opportunities for training and professional development has the project provided?

Post-doctoral researchers Bish, Cuevas-Polo, and graduate students Zhe Cheng and Dionne Argyle were trained in mass spectrometry based proteomics work. This training and their participation in the projects resulted in them being included in publication/manuscript draft 1. and 2. (see above).

How were the results disseminated to communities of interest?

Publication in peer-reviewed journal.

What do you plan to do during the next reporting period to accomplish the goals?

This is the final report.

4. IMPACT

What was the impact on the development of the principal discipline(s) of the project?

Optimization of exosome extraction from cell culture medium. While we have protocols in place that successfully isolate exosomes from medium conditioned by prostate cancer cell lines, and these samples are usable for quantitative proteomics, isolation is difficult, involving depletion of FBS by multiple ultra-centrifugation (UC), prolonged conditioning of the medium (at least one, but even better two days), growth of many cell plates (to obtain at least 100 ml medium), and UC based exosome isolation using sequential centrifugation steps. Future work should explore use of different prostate cancer cell lines to test if they provide a larger yield in exosomes which would simplify the procedure and provide more robust sampling.

The effect of pre-conditioned medium on bone marrow cells and osteoblasts. The medium transfer experiments have shown that an effect of secreted molecules (exosomes and other particles) is small, but present in osteoblasts, as is indicated by the increase in expression of a few markers of the pre-metastatic niche compared to controls consisting of medium conditioned by non-metastatic prostate cancer cells. To confirm these results, further protocol optimization and replicate experiments are necessary.

The major hypothesis of this grant was that exosomes secreted by metastatic prostate cancer cells (in comparison to non-metastatic prostate cancer cells) move bone marrow cells / osteoblasts towards formation of the pre-metastatic niche. The results from the experiments presented here are mostly inconclusive with respect to this hypothesis, but suggest that the hypothesis might be true with respect to transformation of osteoblasts.

What was the impact on other disciplines?

With the two publication/manuscript draft, we contribute to the field of cancer proteomics.

Further, our studies provide thorough testing of different approaches to proteomic investigation of cell-line derived exosomes.

What was the impact on technology transfer?

Nothing to report.

What was the impact on society beyond science and technology?

The third product provides mentoring for graduate students and post-doctoral researchers with respect to career choices.

5. CHANGES/PROBLEMS:

As specified in the approved no-cost extension, the project was delayed due to loss of key personnel (Dr. Bish in June 2014, replaced by Dr. Cuevas-Polo in May 2015, paid from other funds) and medical leave of the PI (May-August 2014). The PI's medical issues (brain tumor) have been completely resolved, but she received one-year extension of the tenure assessment period to account for the temporarily reduced productivity.

The new post-doctoral researcher (Dr. Cuevas-Polo) worked with two students (Zhe Cheng, graduate student; Dionne Argyle, Master's student) to produce two publications (one published, another one in preparation).

Additional challenges were posed by the experimental system, as explained in Section 3.

6. PRODUCTS

Journal publications

Relevance to this grant proposal: products 1 and 2 involve personnel paid (in part) from this grant. They provide essential steps towards robust proteomic characterization of cell line samples, as is required by aims 1 and 2 of this grant. However, they address different systems than prostate cancer.

1. Bish R, Cuevas-Polo N, Cheng Z, Hambardzumyan D, Munschauer M, Landthaler M, Vogel C. Comprehensive Protein Interactome Analysis of a Key RNA Helicase: Detection of Novel Stress Granule Proteins. Biomolecules. 2015 Jul 15;5(3):1441-66. doi: 10.3390/biom5031441. http://www.ncbi.nlm.nih.gov/pubmed/26184334
2. Cuevas-Polo N, Vo D, Qiao M, Choi H, Anant S, Penalva LO, Vogel C. Integrative proteomics analysis of the relationship between the RNA-binding Musashi 1 and miR124. *Under preparation*
3. Vogel C. Systems Approaches to the Eukaryotic Stress Response. PLoS Comp Biology. 2016 Mar 10;12(3):e1004757. doi: 10.1371/journal.pcbi.1004757. http://www.ncbi.nlm.nih.gov/pubmed/26963258

Master's dissertation

Dionne Argyle. The Exosome Chronicles: Towards Unlocking the Mystery of the Pre-Metastatic Niche. New York University, 2015

4. PARTICIPANTS & OTHER COLLABORATING ORGANIZATIONS

What individuals have worked on the project?

Name:	Christine Vogel
Project Role:	PI
Research Identifier:	ORCID 0000-0002-2856-3118
Nearest person month worked:	0.25 months / year
Contribution to Project:	Overall project management, experimental design, writing of manuscripts.
Funding Support:	NYU, NIH R01, this grant – 0.25 months / year

Name:	Rebecca Bish-Cornelissen
Project Role:	Post-doctoral researcher
Research Identifier:	
Nearest person month worked:	4 months total

Contribution to Project:	Dr. Bish established the project and started culturing the respective cell lines
Funding Support:	4 months this grant; NYU (Vogel's startup)

Name:	Dionne Argyle
Project Role:	Master student
Research Identifier:	
Nearest person month worked:	8 months total, 10 hrs/week
Contribution to Project:	Dionne conducted the medium transfer experiments
Funding Support:	6 months this grant

Name:	Zhe Cheng
Project Role:	Graduate student
Research Identifier:	
Nearest person month worked:	5.5 months
Contribution to Project:	Zhe Cheng contributed to experimental work.
Funding Support:	5.5 months; 6.5 months other sources (Vogel's NIH R01)

Has there been a change in the active other support of the PD/PI(s) or senior/key personnel since the last reporting period?

Nothing to report.

What other organizations were involved as partners?

Nothing to report.

5. APPENDICES

Total: 4

A. References
B. Curriculum Vitae – Christine Vogel (PI)
C. Product (published)
D. Manuscript (in preparation, unpublished)

A. References

1. Hendriksen, P.J., et al., Evolution of the androgen receptor pathway during progression of prostate cancer. Cancer Res, 2006. 66(10): p. 5012-20.
2. Peinado, H., et al., Melanoma exosomes educate bone marrow progenitor cells toward a pro-metastatic phenotype through MET. Nat Med, 2012. 18(6): p. 883-91.
3. Eichelbaum, K. and J. Krijgsveld, Combining pulsed SILAC labeling and click-chemistry for quantitative secretome analysis. Methods Mol Biol, 2014. 1174: p. 101-14.
4. Zubiri I, Vivanco F, Alvarez-Llamas G. Proteomic analysis of urinary exosomes in cardiovascular and associated kidney diseases by two-dimensional electrophoresis and LC-MS/MS. Methods Mol Biol. 2013;1000:209-20. doi: 10.1007/978-1-62703-405-0_16.

B. Christine Vogel (PI) – Curriculum Vitae

BIOGRAPHICAL SKETCH

NAME: Christine Vogel
eRA COMMONS USER NAME: CV31.NYU
POSITION TITLE: Assistant Professor
EDUCATION/TRAINING
INSTITUTION AND LOCATION DEGREE

Friedrich-Schiller-University Jena, Germany	B.S. / Master	1995-2000	Biochemistry, cum laude
University College London, United Kingdom	M.Res	2001	Mathematical Biology
University of Cambridge, United Kingdom	PhD	2001-2004	Comp. Structural Biology
University of Texas at Austin, USA	Post-doc	2005-2008	Systems Biology
University of Texas at Austin, USA	Res. Assoc.	2008-2010	Computational Proteomics

A. Personal Statement

My laboratory is interested in the regulation of protein expression in eukaryotic cells responding to environmental stress. To do so, we combine proteome-wide mass spectrometry with computational and statistical models and orthogonal large-scale approaches (such as mRNA sequencing and ribosome footprinting), and have published extensively on the subject of protein quantitation (Nature Biotech 2007, Nature Protocols 2008) and integration with other omics datasets (J Prot Res 2014). We have gained substantial expertise and international reputation in understanding the relationship between protein and mRNA expression levels under steady-state conditions (Mol Sys Bio 2010 and 2016, Nature Reviews Genetics 2012, Science 2013), and we are now exploring the same for dynamically changing systems (Mol Cell Proteomics 2012). Recently, we identified a new stress-protective role for a variant of protein ubiquitination and are working on extensions of the studies (Nature Structural & Molecular Biology 2015).

B. Positions and Honors

Positions and fellowships

1997 – 2000	Fellowship, German National Merit Foundation (Jena, Germany)
2000 – 2001	Research fellowship, German Academic Exchange Organization (London, UK)
2001 – 2004	Pre-doctoral fellowship, Boehringer Ingelheim Foundation (Cambridge, UK)
2002 – 2004	Student fellowship, Medical Research Council (Cambridge, UK)
2004 (life)	Honorary fellowship, LMB Newton Cambridge / European Trust (Cambridge, UK)
2005 (declined)	Post-doctoral fellowship, German Academic Exchange Organization (Austin, USA)
2005 – 2008	Long-term fellowship, International Human Frontier Science Program (Austin, USA)
2008 - 2010	Research Associate, with Prof. Edward Marcotte (Austin, USA)
2011 - date	Assistant Professor, New York University, Ctr. for Genomics and Systems Biology (NY, USA)

Honors

2004 (life)	Member, Trinity College Cambridge (Cambridge, UK)
2009	Young Investigator Award, HUPO, Toronto, Canada
2011	Vivian G. Prins Global Scholar of New York University

Professional activities (selected)
NSF Grant Review Panel Member, 2014 – present; ASTAR Singapore Scientific Reviewer, 2014; Associate Editor, PLOS Computational Biology, 2007 – present; Associate Faculty Member with Prof. E. Marcotte, Faculty1000,

2008 – present; Invited expert panelist during AAAS Science webinar, 2009; Ad hoc reviewer for Cell, Nature Genetics, Science, etc.

Speaker invitations (selected)
2015: Gordon Research Conference on Oxidative Stress & Disease, Ventura CA; Keystone Meeting on Quantitative Proteomics, Stockholm, Sweden; 2014: Systems Biology Meeting at EMBL, Heidelberg, Germany; Weill Cornell Medical College, Seminar Series; 2013: DICP symposium for "Novel techniques for quantitative proteome analysis", Dalian, China (Chinese Academy of Science); Annual Meeting of the Korean Society for Molecular and Cellular Biology (KSMCB), Seoul, Korea; ICCB, Yansei University, Seoul, Korea

C. Peer-reviewed Publications (last 5 years, chronological order)

1. Vogel C, Abreu Rde S, Ko D, Le SY, Shapiro BA, et al. Sequence signatures and mRNA concentration can explain two-thirds of protein abundance variation in a human cell line. Molecular Systems Biology. 2010; 6:400. PubMed [journal] PMID: 20739923, PMCID: PMC2947365

2. Laurent JM, Vogel C, Kwon T, Craig SA, Boutz DR, et al. Protein abundances are more conserved than mRNA abundances across diverse taxa. Proteomics. 2010; 10(23):4209-12. NIHMSID: NIHMS265829 PubMed [journal] PMID: 21089048, PMCID: PMC3113407

3. Vogel C. Translation's coming of age. Molecular Systems Biology. 2011; 7:498. PubMed [journal] PMID: 21613985, PMCID: PMC3130562

4. Kwon T, Choi H, Vogel C, Nesvizhskii AI, Marcotte EM. MSblender: A probabilistic approach for integrating peptide identifications from multiple database search engines. Journal of Proteome Research. 2011; 10(7):2949-58. NIHMSID: NIHMS292806 PubMed [journal] PMID: 21488652, PMCID: PMC3128686

5. Vogel C, Silva GM, Marcotte EM. Protein expression regulation under oxidative stress. Molecular & cellular proteomics: MCP. 2011; 10(12):M111.009217. PubMed [journal] PMID: 21933953, PMCID: PMC3237073

6. Vogel C, Marcotte EM. Label-free protein quantitation using weighted spectral counting. Methods in molecular biology (Clifton, N.J.). 2012; 893:321-41. NIHMSID: NIHMS395003 PubMed [journal] PMID: 22665309, PMCID: PMC3654649

7. Vogel C, Marcotte EM. Insights into the regulation of protein abundance from proteomic and transcriptomic analyses. Nature Reviews Genetics. 2012; 13(4):227-32. NIHMSID: NIHMS395043 PubMed [journal] PMID: 22411467, PMCID: PMC3654667

8. Vo DT, Subramaniam D, Remke M, Burton TL, Uren PJ, et al. The RNA-binding protein Musashi1 affects medulloblastoma growth via a network of cancer-related genes and is an indicator of poor prognosis. The American journal of pathology. 2012; 181(5):1762-72. PubMed [journal] PMID: 22985791, PMCID: PMC3761132

9. Zhou L, Zhang AB, Wang R, Marcotte EM, Vogel C. The proteomic response to mutants of the Escherichia coli RNA degradosome. Molecular BioSystems. 2013; 9(4):750-7. NIHMSID: NIHMS445443 PubMed [journal] PMID: 23403814, PMCID: PMC3709862

10. Kuersten S, Radek A, Vogel C, Penalva LO. Translation regulation gets its 'omics' moment. Wiley interdisciplinary reviews. RNA. 2013; 4(6):617-30. NIHMSID: NIHMS473985 PubMed [journal] PMID: 23677826, PMCID: PMC3797170

11. Vogel C. Evolution. Protein expression under pressure. Science (New York, N.Y.). 2013; 342(6162):1052-3. PubMed [journal] PMID: 24288321

12. Teo G, Vogel C, Ghosh D, Kim S, Choi H. PECA: a novel statistical tool for deconvoluting time-dependent gene expression regulation. Journal of proteome research. 2014; 13(1):29-37. PubMed [journal] PMID: 24229407

13. Gerster S, Kwon T, Ludwig C, Matondo M, Vogel C, et al. Statistical approach to protein quantification. Molecular & cellular proteomics: MCP. 2014; 13(2):666-77. PubMed [journal] PMID: 24255132, PMCID: PMC3916661

14. Bish R, Vogel C. RNA binding protein-mediated post-transcriptional gene regulation in medulloblastoma. Molecules and cells. 2014; 37(5):357-64. PubMed [journal] PMID: 24608801, PMCID: PMC4044306

15. Kwon T, Huse HK, Vogel C, Whiteley M, Marcotte EM. Protein-to-mRNA ratios are conserved between Pseudomonas aeruginosa strains. Journal of proteome research. 2014; 13(5):2370-80. PubMed [journal] PMID: 24742327, PMCID: PMC4012837

16. Tchourine K, Poultney CS, Wang L, Silva GM, Manohar S, et al. One third of dynamic protein expression profiles can be predicted by a simple rate equation. Molecular BioSystems. 2014; 10(11):2850-62. NIHMSID: NIHMS621486 PubMed [journal] PMID: 25111754, PMCID: PMC4183714

17. Silva GM, Finley D, Vogel C. K63 polyubiquitination is a new modulator of the oxidative stress response. Nature Structural & Molecular Biology. 2015; 22(2):116-23. NIHMSID: NIHMS649187 PubMed [journal] PMID: 25622294, PMCID: PMC4318705

18. Bahrami-Samani E, Vo DT, de Araujo PR, Vogel C, Smith AD, et al. Computational challenges, tools, and resources for analyzing co- and post-transcriptional events in high throughput. Wiley interdisciplinary reviews. RNA. 2015; 6(3):291-310. NIHMSID: NIHMS640467 PubMed [journal] PMID: 25515586, PMCID: PMC4397117

19. Bish R, Cuevas-Polo N, Cheng Z, Hambardzumyan D, Munschauer M, et al. Comprehensive Protein Interactome Analysis of a Key RNA Helicase: Detection of Novel Stress Granule Proteins. Biomolecules. 2015; 5(3):1441-66. PubMed [journal] PMID: 26184334, PMCID: PMC4598758

20. Silva GM, Vogel C. Mass spectrometry analysis of K63-ubiquitinated targets in response to oxidative stress. Data in brief. 2015; 4:130-4. PubMed [journal] PMID: 26217776, PMCID: PMC4510443

21. McManus J, Cheng Z, Vogel C. Next-generation analysis of gene expression regulation - comparing the roles of synthesis and degradation. Molecular BioSystems. 2015; 11(10):2680-9. NIHMSID: NIHMS715555 PubMed [journal] PMID: 26259698, PMCID: PMC4573910

22. Bowling H, Bhattacharya A, Zhang G, Lebowitz JZ, Alam D, et al. BONLAC: A combinatorial proteomic technique to measure stimulus-induced translational profiles in brain slices. Neuropharmacology. 2016; 100:76-89. NIHMSID: NIHMS720555 PubMed [journal] PMID: 26205778, PMCID: PMC4584208

23. Cheng Z, Teo G, Krueger S, Rock TM, Koh HWL, Choi H, Vogel C. Differential dynamics of the mammalian mRNA and protein expression response to misfolding stress. Molecular Systems Biology. In press.

24. Vogel C. Systems Approaches to the Eukaryotic Stress Response. PLoS Comp Biology. 2016 Mar 10;12(3):e1004757. doi: 10.1371/journal.pcbi.1004757. http://www.ncbi.nlm.nih.gov/pubmed/26963258

My Bibliography Link
http://www.ncbi.nlm.nih.gov/sites/myncbi/1J_Xgvc-U-D5w/bibliography/40556229/public/?sort=date&direction=ascending

C. Product (published)

See PDF at end

D. Manuscript (in preparation)

Integrative proteomics analysis of the relationship between the RNA-binding Musashi 1 and miR124

Alternative: Identification of targets of the RNA binding protein Musashi-1 (MSI1) in medulloblastoma

Nerea Cuevas-Polo[1], Dat Vo[2,3], Mei Qiao[2,7], Hyungwon Choi[4], Shrikant Anant[2,5], Luiz Penalva[2,7], and Christine Vogel[1*]

1. New York University, Center for Genomics and Systems Biology, New York NY USA.
2. Greehey Children's Cancer Research Institute, University of Texas Health Science Center, San Antonio, Texas USA
3. Department of Cellular and Structural Biology, University of Texas Health Science Center, San Antonio, Texas USA
4. Saw Swee Hock School of Public Health, National University of Singapore and National University Health System, MD3, 16 Medical Drive, 117579 Singapore
5. Department of Molecular and Integrative Physiology, University of Kansas Medical Center, Kansas City, Kansas USA
6. University of Kansas Cancer Center, Kansas City, Kansas USA
7. Cancer Therapy and Research Center, University of Texas Health Science Center, San Antonio, Texas USA

* Address correspondence to: Christine Vogel (cvogel@nyu.edu)

Keywords:

Musashi-1, Musashi1, MSI1, medulloblastoma, brain tumor, xenograft, proteomics, mass spectrometry, RNA binding protein, post-transcriptional regulation, miR-124

Abstract:

Musashi1 (MSI1) is an RNA binding protein with a key role in the development of the central nervous system. MSI1 is – if aberrantly expressed – directly linked to formation of medullo- and glioblastoma. Despite these important roles, identification of its mRNA targets and regulatory mechanism has proven extremely challenging. To address this issue, we collected multiple proteomics datasets of MSI knockdown, i.e. one xenograft and two cell line models, and integrated these with orthogonal information in an unbiased, but focused way. Doing so, we identified 15 and 6 new potential MSI1 targets that are translationally repressed or activated respectively. The set of translation repressed MSI1 targets overlapped significantly with validated targets of miR124 which is also involved in neuronal development, but absent in medullo- and glioblastoma. The mRNAs of two of these proteins – DHCR24 and PTRF – are directly bound by the MSI1 protein, as reported by published assays. Neither of the two proteins have been linked to MSI1 function. Overexpression of miR124 validated a functional connection between the miRNA miR124 and RNA-binding protein MSI1 in the neuronal cell system. It confirmed a model in which translation of DHCR24 and PTRF is repressed by MSI1 and possibly miR124 – suggesting a model for normal cells and tumor formation.

Introduction

Organisms have evolved an astounding array of mechanisms to regulate gene expression across space and time. Protein concentrations can be manipulated by altering the level of transcription, RNA processing, RNA decay, translation, post-translational protein modification, and protein degradation. Control of transcription is the best-understood regulatory mechanism, due in part to early technological advances such as microarrays which permitted the large scale study of the transcriptome. However, while we know that post-transcriptional gene regulation is also critical for maintaining proteostasis, our understanding of these post-transcriptional mechanisms is far less advanced.

The regulation of protein translation rates by RNA binding proteins is one aspect of post-transcriptional gene regulation which is known to be particularly important in the central nervous system [1, 2]. The importance of proper translational regulation in the CNS is highlighted by the number of neurodegenerative diseases and other neurological disorders which result from dysfunctional protein translation. These pathologies are frequently a direct consequence of mutation of an RNA binding protein. For example, mutation of the translational repressor *fragile X mental retardation 1* (FMR1) results in fragile X syndrome, a developmental disorder which is characterized by significant cognitive impairment [3-5] . In another example, mutation of the genes encoding the RNA binding proteins *fused in sarcoma/translated in liposarcoma* (FUS/TLS) or *TAR DNA-binding protein 43* (TDP-43) results in the neurodegenerative disorder amyotrophic lateral sclerosis (ALS) [6-10]. Mutations in RNA binding proteins have also been implicated in oncogenesis. Somatic overexpression of *cytoplasmic polyadenylation element-binding protein 4* (CPEB4) has been linked to both pancreatic ductal adenocarcinoma and glioblastoma, due to the translational re-activation of mRNAs which are normally silenced in these tissues [11]. Thus, study of neural RNA binding proteins and their targets is critical both for understanding normal CNS development, and a wide variety of diseases including cancer.

Musashi1 (MSI1) is one member of a family of RNA binding proteins with diverse functions in the central nervous system (CNS) [12-15]. Roles for MSI1 in asymmetric cell division, stem cell function and cell fate were first characterized in *Drosophila*, and soon thereafter extended to mammalian MSI1 homologs in mouse and human [16-19]. Mammalian MSI1 is expressed selectively in neural stem/progenitor cells, as well as in certain other stem cell populations, and serves to maintain the proliferation and renewal of these cells [19-23]. As neuronal progenitor cells differentiate, MSI1 expression gradually decreases [15].

Given its importance in CNS development and prominent expression in neural stem cells, it is not surprising that MSI1 has been linked to several types of brain tumors, including glioblastoma and medulloblastoma. MSI1 is overexpressed in many different brain tumors, including medulloblastoma, glioma, and ependymoma [24-26]. The parallels between the role for MSI1 in normal development and cancer is particularly intriguing in the case of medulloblastoma, a brain tumor originating in the cerebellum whose cells closely resemble neural stem/progenitor cells in terms of appearance, marker expression, and differentiation potential [27, 28]. High MSI1 expression in both glioblastoma and medulloblastoma correlates with poor patient prognosis [29, 30]. No somatic mutations of MSI1 have been identified in the large medulloblastoma sequencing studies, suggesting that its oncogenic role may instead be achieved through overexpression of wild-type MSI1 protein [31-34]. In some cases, this overexpression may be due to copy number gain in the area of chromosome 12q24, which has been observed in several studies but not yet characterized in terms of MSI1 expression [35, 36].

Numerous lines of evidence support the hypothesis that MSI1 plays an oncogenic role in medulloblastoma. MSI1 is required for the formation and maintenance of neurospheres by medulloblastoma cells, suggesting a role for MSI1 in cancer stem cell proliferation, self-renewal, and/or multipotency [37, 38]. Analyses of downstream pathways in brain tumor cells reveal that MSI1 activates Notch and PI(3) kinase-Akt signaling [37]. Inhibition of MSI1 in mouse models of medulloblastoma, glioblastoma, and colorectal cancer has been demonstrated to reduce tumor size and increase overall survival, highlighting the key oncogenic role played by MSI1 in these tumors [30, 37, 39].

The key unanswered question then is precisely how MSI1 exerts its oncogenic effect in medulloblastoma. In general, MSI1 influences cellular phenotypes by post-transcriptional regulation of the expression level of a number of target genes. MSI1, which binds RNA via two tandem RNA recognition motifs (RRM), preferentially binds the sequence (G/A)U_{1-3}AGU, which is often found as repeats in the 3'untranslated region (3'UTR) of target mRNAs [30, 40]. Upon binding, MSI1 can up- or down-regulate translation, although MSI1 is generally considered to be a

translational repressor [12, 41]. The most well-characterized pathway targeted MSI is Notch signaling, which is enhanced via MSI1-mediated translational repression of Numb, which functions to repress this pathway [40]. Other individual genes which have been shown to be targets of translational regulation by MSI1 include CDKN1A, doublecortin, and Robo3 [12, 14, 40, 42].

A number of efforts have been undertaken to identify novel targets of MSI1 regulation via large-scale characterization of the mRNAs bound by MSI1 via reverse-immunoprecipitation experiments (RIP-CHiP and iCLiP). These experiments resulted in the identification of mRNAs bound by MSI1 in a number of different cell lines from different origins, including U251 glioblastoma and the Daoy medulloblastoma cell line [30, 43]. These results indicate that MSI1 potentially regulates hundreds or thousands of targets, influencing such critical cellular processes as proliferation, differentiation, and apoptosis [30, 38]. However, to date, such large scale experiments have examined MSI1 targets only at the level of mRNA binding.

MSI1 interacts with AGO2 [44], which is required for RNA-mediated gene silencing recruiting miRNAs and siRNAs through a complex process [45]. Emerging studies have shown that miRNAs are involved in the malignant progression of cancer [46, 47]. miRNAs, a class of post-transcriptional regulators, are short noncoding RNAs (~22 nucleotides) that bind to the complementary sequences in the 3′-UTRs of multiple mRNA transcripts, thereby resulting in the silencing of target genes. microRNAs have fundamental importance in normal development, differentiation, growth control and in human diseases such as cancer [46, 47]. Moreover, mir-124 is known to be involved in regulate the differentiation of embryonic stem cells and/or neurogenesis [48, 49]. miR-124 is significantly down-regulated in glioblastoma samples compared with non-tumor brain tissues [50-52], suggesting that miR-124 may play a critical role in brain tumorigenesis and progression.

Bioinformatic searches have predicted more than one thousand RBPs (1542) [53], and almost double that number of miRNAs (2588) in the human genome [54]. Due to their vast numbers, computational analysis predicted substantial combinatorial control of mRNA fates through simultaneous assembly of RBPs and miRNAs on particular mRNAs (e.g., [55]). Thus, looking at single proteins or the action of distinct miRNAs on mRNA fates alone could be misleading, as it does not consider the entire arrangement of trans-acting regulatory factors that affect specific mRNAs. Moreover, the differential expression of RPBs and miRNAs can lead to condition-specific assemblies restricted to particular cell-types or subcellular compartments. Some examples support the notion of extensive combinatorial post-transcriptional control of mRNA stability and of translation through interactions with RBPs and/or miRNAs [56]. Recent mechanistic studies exemplify antagonistic or synergistic arrangements of: (i) RBPs and miRNAs; (ii) RBPs and RBPs and (iii) miRNAs on cytoplasmic mRNAs and their impact in cell biology [56].

It is known that miRNAs can work in concert to enhance the inhibition of expression of a mRNA target [57, 58]. Different pools of miRNAs may possess the ability to target a given transcript simultaneously, but in reality, this depends on the presence of the miRNAs in the same place at the same time, and miRNA expression is not uniformly distributed within different tissues and tumours [57, 58].

FXR1 is a key regulator of tumor progression [59]. In coordination with the Argonaute 2 protein, FXR1 associates with certain elements of tumor-necrosis factor α [60]

In this study, we identify proteins whose expression levels change upon MSI1 inhibition. We then incorporate other –omics-level datasets into our analysis of these MSI1 targets in order to identify genes which may play a key role in carrying out the oncogenic role of MSI1 in medulloblastoma and glioblastoma. Here we also suggest a combinatorial action between MSI1 and miR124.

Result

Proteomics analysis of MSI1 knockdown experiments

To better understand the range of proteins regulated by MSI1, we set up an experiment to identify proteins whose expression levels are altered after MSI1 knockdown in a mouse xenograft model of medulloblastoma. The samples were obtained from an experiment described in a previously published study [30]. Briefly, xenograft tumors composed of human Daoy medulloblastoma cells were grown in the flanks of nude mice. After the tumors were established and palpable, the tumors were directly injected with one of three solutions: a vehicle control, a scrambled siRNA, or a siRNA targeted against MSI1. Injection of MSI1 siRNA caused significant MSI1 knockdown at the RNA and protein level, and resulted in substantial inhibition of tumor growth [30] confirming that MSI1 plays a crucial role in medulloblastoma formation.

To identify proteins whose expression levels were altered by MSI1 knockdown in these tumors, we harvested three tumors each from the scramble siRNA and MSI1 siRNA groups. Each sample was analyzed in triplicate by shotgun LC-MS/MS analysis. The Daoy xenograft experiment (D-X) was complemented by two conceptually similar proteomics experiments in which MSI1 was knocked down in the Daoy (D-CL) and U251 (U-CL) cell lines (D-CL and U-CL, respectively; **Figure 1A,B**). All proteomics files were carefully filtered to obtain high-quality datasets, resulting in 3,014 human protein groups identified from the xenograft Daoy medulloblastoma tumors, and 1,195 and 1,891 proteins from the Daoy medulloblastoma and U251 glioblastoma cell line, respectively (**Table S1, Figure SXXX, Supplementary Datasets S1-3**).

As RNA-binding proteins often cause small expression changes **REFS**, we extracted differentially expressed proteins based on comparatively loose cutoffs which we analyzed for overlap across the xenograft and cell line models (**Figure 2A**). The overlap between up-regulated proteins in the medulloblastoma xenograft and the medulloblastoma cell line was significant (hypergeometric text, p-value<0.05, see **Figure SXXX**), supporting the quality of the proteomics data. Only five and two up- and down-regulated proteins, respectively, were common to across three datasets. We extracted 96 and 61 proteins that were up- and down-regulated, respectively, in at least two of the three proteomics datasets (**Figure 2B,C**). The proteins were enriched in functions related to protein synthesis and fatty acid elongation (**Figure 2D**). These proteins were used for further analysis and are henceforth referred to as the up- or down-regulated proteins (upon MSI1 knockdown).

Integration with mRNA binding data

We next characterize the differentially expressed proteins as to whether they are likely to be directly or indirectly regulated by MSI1. “Direct regulation” implies that MSI1 binds to the mRNA for a particular gene, thereby altering the protein expression level (most likely through regulation of translational efficiency). In contrast, “indirect regulation” describes a scenario where, for example, a protein’s expression level is altered because it is downstream of a protein whose expression is directly regulated by MSI1. To extract candidates for direct MSI1 regulation, we made use of three RIP-CHiP [30] and iCLIP datasets [61] that describe the set of mRNAs bound to MSI1. The intersection between the set of mRNAs bound by MSI1 and our proteomics experiments shows that 15 up- and six down-regulated proteins have mRNAs that are bound by MSI1 (**Table 1**, **Figure 3A,B**). These proteins are considered putative direct targets of MSI1, and indeed, eleven of the 21 proteins have functions consistent with cancer or cell proliferation (**Table 1**), supporting their involvement in MSI1 based tumorigenesis. The intersection for up-regulated proteins is significant (p-value=0.008), while the intersection for down-regulated proteins is not (p-value=0.44). Therefore we focused further studies on the 15 up-regulated direct targets.

Combinatorial action between MSI1 and miR124

Based on several lines of evidence, we hypothesized combinatorial actions of MSI1 and the micro-RNA miR124. For example, MSI1 is known to interact with AGO2 (**Figure SXXX**), which is an RNA binding protein that enables microRNA based translation repression. Further, miR124, together with miR34 and miR18, are aberrantly expressed in both glio- and medulloblastoma (**Figure SXXX**), rendering them prime candidates for their targeting similar proteins. We focus here on miR124; other results are shown in **Figure SXXX**.

To test if MSI1 and miR124 regulate similar target mRNAs, we intersected the list of miR124 targets with the up-regulated proteins obtained from our study (**Figure 3C, D**). THE MIR124 TARGETS WERE TAKEN FROM A PUBLIC REPOSITORY AND HAVE WEAK EXPERIMENTAL EVIDENCE, I.E. MICROARRAY. WE FIND A TOAL OF 112 MI124 TARGETS AMONGST THE 2,000 PROTEINS. Both the proteomics data only, and the

combined data of the 15 direct MSI1 targets overlap with miR124 targets significantly (p-value=0.0008 and p-value=0.004, respectively) suggesting that indeed, the RNA-binding protein and the miRNA have a direct functional relationship. That this relationship is not entirely due the two regulators targeting similar pathways of proteins is illustrated by the finding that the function enrichments of the target datasets are different for the proteomics data (**Figure 2D**) and the miR124 targets (*not shown*).

If MSI1 impacts miR124 expression in a direct or indirect way, the miRNA's expression should be change in the MSI1 knockdown experiment. Indeed, we find that miR124 expression increases as predicted in the MSI1 knockdown (**Figure 4A**), consistent with a model in which the MSI1 knockdown moves the cell towards the non-cancerous, normal state in which miR124 is expressed (**Figure 6A,C**).

Overexpressing miR124

In comparison to the above knockdown experiment, upon miR124 overexpression in the U251 glioblastoma cell line, MSI1 expression did not change (**Figure 4B**). This finding supports a model in which MSI1 negatively affects miR124 expression, either directly (through binding to the miR124 RNA) or indirectly (via other proteins), but miR124 does not affect MSI1 (**Figure 6B**).

Using quantitative proteomics, we analyzed a fraction of the proteome in response to miR124 overexpression (**Figure 5A**). With similar cutoffs as for the xenograft data, we identified 400 proteins that were down-regulated in the overexpression experiment compared to control. Since micro-RNAs mostly suppress translation, we focused on this set of proteins as these are putative direct targets of miR124. They are significantly enriched in functions of developmental growth (p-value=0.0008). However, the proteins down-regulated under miR124 overexpression do neither overlap significantly with MSI1 activated nor with the MSI1 suppressed proteins (**Figure 5B**).

DISCUSS HEATMAP – ANYONE INTERESTING THERE? DISCUSS THAT MANY UPREGULATED PROTEINS, BUT FOR PURPOIOSE OF PAPER ONLY DOWNREGULATED ONES (MIRNA FUNCTION)

DHCR24 and PTRF

Finally, we examined DHCR24 and PTRF further, as these two proteins at the center of the regulatory scenarios considered here (**Figure** 3D): they are miR124 targets as reported in the databases, in the up-regulated proteomics dataset (MSI1 knockdown) and their mRNA is bound by MSI1. The two proteins have suggested roles in cell proliferation, but have otherwise not been described to link to brain tumors or MSI1 and miR124 function (**Table 1**).

We tested the hypothesis that DHCR24 and PTRF are indeed regulated by both MSI1 and miR124. As described above, both proteins are up-regulated in the MSI1 knockdown and their mRNA is bound by MSI1, suggesting that MSI1 directly suppresses translation of DHCR24 and PTRF. DHCR24 even has the MSI1 binding motif in its 3'UTR (**Table 1**). However, despite repression by MSI1, and MSI1's presence in glioblastoma cells, the two proteins are not completely repressed, but still present at measurable levels (**Figure 5B, 6A**). Upon overexpression of miR124, DHCR24 decreases in expression, suggesting that its mRNA is a target of the micro-RNA and is repressed in its translation (**Figure 5A**).

One might asked why then the protein's translation is not also repressed in the MSI1 knockdown cells, as miR124 is upregulated in these cells as well. Two reasons occur. One, the expression level of miR124 upon MSI1 knockdown might be much lower than that of the artificially overexpressed miR124, and hence have only a minor repressive effect. And two, the absence of MSI1 counteracts the repressive role of miR124 as expression of DHCR24 and PTRF now increases.

Discussion

Many putative MSI1 targets function in cell proliferation

Musashi-1 (MSI1) is an RNA-binding protein that is highly expressed in both medullo- and glioblastoma and activates or represses translation of target proteins (**Figure 1A**). Importantly, when MSI1 is knocked down, tumor size and other cancer properties of the cells are drastically reduced [30], placing the protein into an important position with respect to tumorigenesis. Despite this crucial role, only four direct MSI1 targets are known today **[62]**.

Based on background, we investigated the proteomics response to MSI1 knockdown in three independent expression datasets in a xenograft and medullo- and glioblastoma cell line models. More than 3,000 proteins were quantified across six replicate xenografts in MSI1 knockdown and control mice, providing a comprehensive dataset that was complemented by the smaller cell line analyses. Overall, the expression fold change was small, with an

average maximum change of 13 and 11 fold change for the up- and downregulated proteins respectively (**Figure 2A**). This finding is consistent with other studies that identified both RNA-binding proteins and miRNAs to have only small effects on protein expression fold changes and might fine-tune expression levels rather than cause major regulatory changes **REF**.

As the proteins changing in the MSI1 knockdown experiments can be both directly and indirectly regulated by MSI1, we combined the proteomics data with published experimental information on mRNAs bound by MSI1 (**Figure 3A,B**). Again, these data were derived from integration of multiple independent studies. If a protein changes in its expression level upon MSI1 knockdown and its mRNA is bound by MSI1, then it might be a direct target. Using this approach, we identified 21 putative MSI1 targets whose translation is directly regulated in either negative (15) or positive (6) direction (**Table 1**). More than half of these proteins (11) are involved in cancer or cell cycle regulation, supporting the notion that they might indeed be direct MSI1 targets. Notably, the intersection was significant for translation-repressed proteins (p-value=0.016), but not for translation-activated proteins (p-value=0.44) suggesting that in this context MSI1 primarily acts as a translation repressor.

MSI1 and miR124 are likely functionally linked

Both RNA-binding proteins and miRNAs affect translation, and a few studies suggest that the two independent pathways act in a combinatorial manner on joined target mRNAs **REF**. Such combinatorial action delivers one explanation for the small effects observed when any individual regulator is perturbed or the lack of overlap amongst the knockdown experiments or mRNA binding experiments. As MSI1 has a confirmed protein-protein interaction with AGO2, the main protein involved in miRNA function, we explored a possible functional relationship of MSI1 and micro-RNAs.

We focused this study on miR124 for several reasons. miR124 is down-regulated in several types of mammalian cancer [63-65], miR124, miR18, and miR33 were the only three miRNAs which were listed to have regulatory roles in both glio- and medulloblastoma (**Figure SXXX, [66, 67]**). miR33 did not have targets in our datasets, and the results for miR18a are discussed in the **Figure SXX**. miR124 has an important role in regulating growth, invasiveness, stem-like traits, differentiation and apoptosis of glioblastoma cells [68, 69] – all functions relevant to this study's context. Further, similar to MSI1, miR124 is also known to be involved in neuronal development, specifically during XXX **REF**. Finally, our proteomics data shows that MSI1 represses the translation of FXR1 which in turn is a regulator of miR124 [70], suggesting that if not directly, then MSI1 might indirectly affect miR124 function.

We conducted a number of tests that confirmed this putative functional anti-correlation between MSI1 and miR124 (**Figure 6B**). First, we observed a significant overlap between miR124 mRNA targets with proteins repressed by MSI1 as identified in our study (**Figure 3C**, p-value=0.0008). However, as this intersection might simply be due to the two regulators acting in similar functional spaces, we performed experiments that investigated mutual dependence of MSI1 and miR124 on each other. These experiments showed that miR124 expression indeed increases in an MSI1 knockdown (**Figure 4A**), but *vice versa*, MSI1 expression levels are not affected by overexpression of miR124. Consistently, overexpressing miR124 does not produce a proteomics response that is equivalent to that of MSI1 knockdown (**Figure 5B**) – the miRNA alone has independent effects.

This model enables several outcomes that are subject to future investigations. For example, we predict that miR124 overexpression does not affect tumorigenesis, and using this miRNA alone is not a good anti-cancer strategy. However, since this miRNA is expressed in normal glial and medulla cells, but not the tumor tissue, combinatorial approaches that simultaneously knockdown MSI1 and overexpress miR124 might amplify the beneficial effect that has been observed when MSI1 is knocked down [30]. The combined presence of miR124 and absence of MSI1 might move the cells towards a more complete restoration of the normal phenotype.

Further, our results indicate for the first time that FXR1, an important translation regulator involved in autism and other neurological disorders [71], might have a direct link to brain tumor formation through it being affected by MSI1 and regulating miR124 expression. Future work might investigate the impact of FXR1 knockdown on glio- and medulloblastoma formation and test if the protein's mRNA might be directly regulated by MSI1.

Example case: the regulation of DHCR24 and PTRF

To test the regulatory role of MSI1 on new putative direct targets and a possible functional relationship with miR124 on individual proteins, we selected the strongest candidates from our studies, DHCR24 and PTRF, as these

proteins are affected by MSI1 knockdown, their mRNA is bound by MSI1 protein and miR124. DHCR24 also has an MSI1 binding motif in its 3'UTR. DHCR24 is known to be highly expressed in tumor cells [72], whereas PTRF is involved in lipodystrophy **[73]**, but neither protein has been characterized as an MSI1 or miR124 target.
The proteomics study showed that DHCR24 and PTRF are up-regulated in the MSI1 knockdown experiment compared to tumor cells which suggests that MSI1 might repress translation of the two proteins. In comparison, the overexpression of miR124 decreases DHCR24 expression level and leaves PTRF mostly unchanged (or slightly decreasing). Since MSI1 is also present in the miR124 overexpression sample, the interpretation of the results is difficult. We therefore conclude that DHCR24 and PTRF might be translationally repressed by MSI1, but only be minor targets of miR124 (**Figure 6A**).

Conclusion

Our study highlights the power of combining large datasets from complementary types of experiments -- i.e. proteomics of knockdown and overexpression experiments, protein pulldown and mRNA target analysis, and bioinformatics -- and diverse sample types -- i.e. from tumor xenografts and cancer cell lines --, to provide a rich context with which to evaluate and prioritize candidate genes for follow-up studies. We propose 21 strong new candidates for direct MSI1 regulation (**Table 1**), many of which already have known roles in tumor formation and cell proliferation.
We demonstrate that while a single study is often unable to extract meaningful signals, the integration of the datasets and careful choice of cutoffs allowed us to propose a possible link between the translation regulator MSI1 and miRNA miR124 in a biomedically important system (**Figure 6B**). In normal brain cells, MSI1 is absent, but the miR124 is expressed at medium levels, keeping expression of its targets at functional levels (**Figure 6A**). Upon tumor formation, MSI1 represses the expression of the micro-RNA, but since it also represses DHCR24 and PTRF, their expression levels do not change drastically. However, once MSI1 is knocked-down, the translation of the two proteins is released. Only in the miR124 overexpression experiment, in which both the miRNA and the MSI1 repressor were present, the expression levels of DHCR24 and PTRF decrease.

Materials and Methods

Cell Culture

The Daoy and U251 cell lines were obtained from ATCC (Manassas, VA). Cells were according to ATCC recommendations: they were grown in a humidified incubator at 37°C in 5% carbon dioxide, in Dulbecco's modified Eagle medium (Hyclone, Logan, UT) supplemented with 10% fetal bovine serum (Atlanta Biologicals, Lawrenceville, GA) plus penicillin/streptomycin (Gibco, Gaithersburg, MD).

MSI1 knockdown

Proteomics analysis for the xenograft samples was performed on the same tissue as used for the published study [30]. MSI1 knockdown in U251 and Daoy cell lines was performed as follows… All experiments were performed in triplicate unless specified otherwise.

miRNA overexpression

miR124 was overexpressed in U251 cells using… . All experiments were performed in triplicate.

Protein sample preparation

Cells were pelleted by ultra-centrifugation. Proteins were first reduced using 10mM dithiothreitol (DTT) (final concentration). Reduced cysteine side chains were then alkylated with 50 mM iodoacetamide (IAA) (final concentration) and incubated with trypsin digestion solution at a nominal enzyme to substrate ratio of 1:50 overnight at 37 °C. All samples were cleaned with Aspire C18 desalting tips (Thermo Fisher Scientific, New York, NY, USA) according to the manufacturer's instructions as the final step before mass spectrometry analysis. Desalted peptides were resuspended in 5% acetonitrile/0.1% formic acid.
For the xenograft sample, the flash-frozen tumors were then processed to extract their protein contents for analysis by mass spectrometry. Mouse albumin was removed prior to protein sample processing using the XXX kit from XXX.

Mass spectrometry

Mass spectrometry analysis was performed on an LTQ-Orbitrap Classic (Thermo Electron) coupled to an Eksigent nano-LC Ultra HPLC (Absciex, Framingham, MA, USA). Peptides were separated on 15 cm Agilent ZORBAX 300 StableBond C18 column (75 μm ID, 3.5 μm particle, 300 Å pore size) by reverse-phase chromatography with a

gradient of 5 to 40% acetonitrile over 300 min. Survey full-scan mass spectra were acquired from 300–2000 m/z, with a resolution of 60,000. The top 20 most intense ions from the survey scan were isolated and fragmented in the linear ion trap by collision-induced dissociation (normalized collision energy = 35 eV). The dynamic exclusion list (n = 500) used a retention time of 90 s and a repeat duration of 45 s (repeat count = 1), and preview scan mode was enabled. Ions of charge state = 1 or unassigned charge states were rejected.

Western blotting

Lysates were prepared using RIPA buffer (50 mM Tris pH 7.5, 1% NP40, 0.1% SDS, 0.5% sodium deoxycholate, 150 mM NaCl, one Complete mini protease inhibitor tablet and 1 PhosStop tablet per 10 mL). Equal protein amounts were run on SDS-PAGE gels, transferred via wet electroblotting, and blocked in 5% milk in TBS-T (50 mM Tris pH 7.5, 150 mM NaCl, 0.1% Tween-20). The following primary antibodies were incubated with the blots overnight at a dilution of 1:1000 unless otherwise noted: anti-PTFR (Abcam, Cambridge, United Kingdom, ab48824), anti-MSI1 (Abnova, H00004440-D01), anti-DHCR24 (Cell Signaling Technology, 2033S), ant-βactin (Cell Signaling Technology, 4967S). HRP-conjugated secondary antibodies were used at a dilution of 1:5000 for 1 h (GE Healthcare, Little Chalfont, UK).

Bioinformatics analysis

The acquired RAW mass spectrometry files were loaded into MaxQuant (version 1.3.0.3) and searched against the human UniProtKB database (version 2015_05). The Daoy xenograft dataset was searched against both human and mouse databases. MaxQuant default settings were used for the analysis, except for quantification, where the 'iBAQ' and 'label-free quantification' (LFQ) were selected, and FDR was set to 0.1 both for protein and peptide level. We removed reverse and contaminant proteins and proteins which were identified in fewer than three of the six xenograft samples. For the xenograft dataset, we discarded mouse proteins from further consideration. Proteins for which all peptides were ambiguous as to their human/mouse origin were assumed to be human for the purposes of this study, because in general the abundance of the human proteins far exceeded that of the mouse proteins identified. All mass spectrometry proteomics data have been deposited to the ProteomeXchange Consortium [74] via the PRIDE partner repository (identifier: PXD002964 for MSI1 knockdown and PXD002976 for mir-124) at http:/**XXX**.

To identify differentially expressed proteins, the proteomics datasets from the xenograft MSI1 knockdown and miR124 overexpression were subjected to analysis by qPROT **REF** which is a statistical tool particularly designed for replicate mass spectrometry data. Proteins were considered differentially expressed if changing at least 1.2 fold in their concentration as estimated from their LFQ intensities. The auxiliary proteomics datasets on MSI1 knockdown in the Daoy and U251 cell lines were filtered for 1.2 fold change in LFQ intensities to extract differentially expressed proteins.

The RIP-CHiP and iCLIP data were taken from two published studies [30][48]. The RIP-CHiP experiments were performed in two different cell lines: U251 glioblastoma cells (GSE37216), and Daoy medulloblastoma cells (GSE30904). The iCLIP data was obtained for U251 cells (GSE68800). In each study, an mRNA was defined as bound by MSI1 if its expression level changed more than three-fold in the pulldown – which is a stringent criterium. IN ADDITION, THE iCLIP WAS REQUIRED TO BE with at least 1 site in 3' or 5' UTR in at least 2 replicates – HENCE VERY STRINGENT AND EXPECTED TO HAVE MANY FALSE NEGATIVES

The target lists for the miRNAs were taken from miRTarBase (http://mirtarbase.mbc.nctu.edu.tw/). WE ONLY CONSIDERED TARGETS… MIrTARGBASE REPORTS WEAK EXPERIMENTAL VALIDATION FOR THE MIR124 TARGETS BASED ON MARRAY

Gene names and function annotations were taken from UniprotKB (http://www.uniprot.org). The prediction of the MSI1 recognition motifs in the 3'UTR of the mRNA was taken from MEME Suite (http://meme.ebi.edu.au/meme/db/sequences). The role in cancer formation was estimated based on Uniprot KB and OMIM (http://www.omim.org/). Venn diagrams were generated using the online available tool Venny (http://bioinfogp.cnb.csic.es/tools/venny/). All GO annotations and enrichment analyses were performed using NCBI's David Bioinformatics Suite [75]. Heatmaps were generated with the Perseus tool [76]

Acknowledgements

We thank Rebecca A. Bish for valuable input into the work. C.V. acknowledges funding by the NIH (Ro1 GM113237), the DOD (Hypothesis Testing Award PC121532), NYU Whitehead Foundation, the NYU University Research Challenge Fund, and the Zegar Family Foundation Fund for Genomics Research at New York University.

Figures / Tables

Figure 1: Integrative analysis of the translation regulator Musashi 1

A. General model of translation regulation of a protein X based on proteins and miRNAs binding to its mRNA X, in this case MSI1 and miR124 respectively. **B.** Datasets used in this study, both collected in-house and taken from published work (see text). mRNA.**C.** Blue rectangle - miR124; orange ovals – proteins; blue line – mRNA. **C.** Large-scale proteomics analysis of MSI1 knockdown (KD) in Daoy xenografts in mouse (D-X), the Daoy (D-CL), and U251 cell line (U-CL) using mass spectrometry. White – input samples, light grey – analytical methods, and dark grey – final dataset used for further analysis.

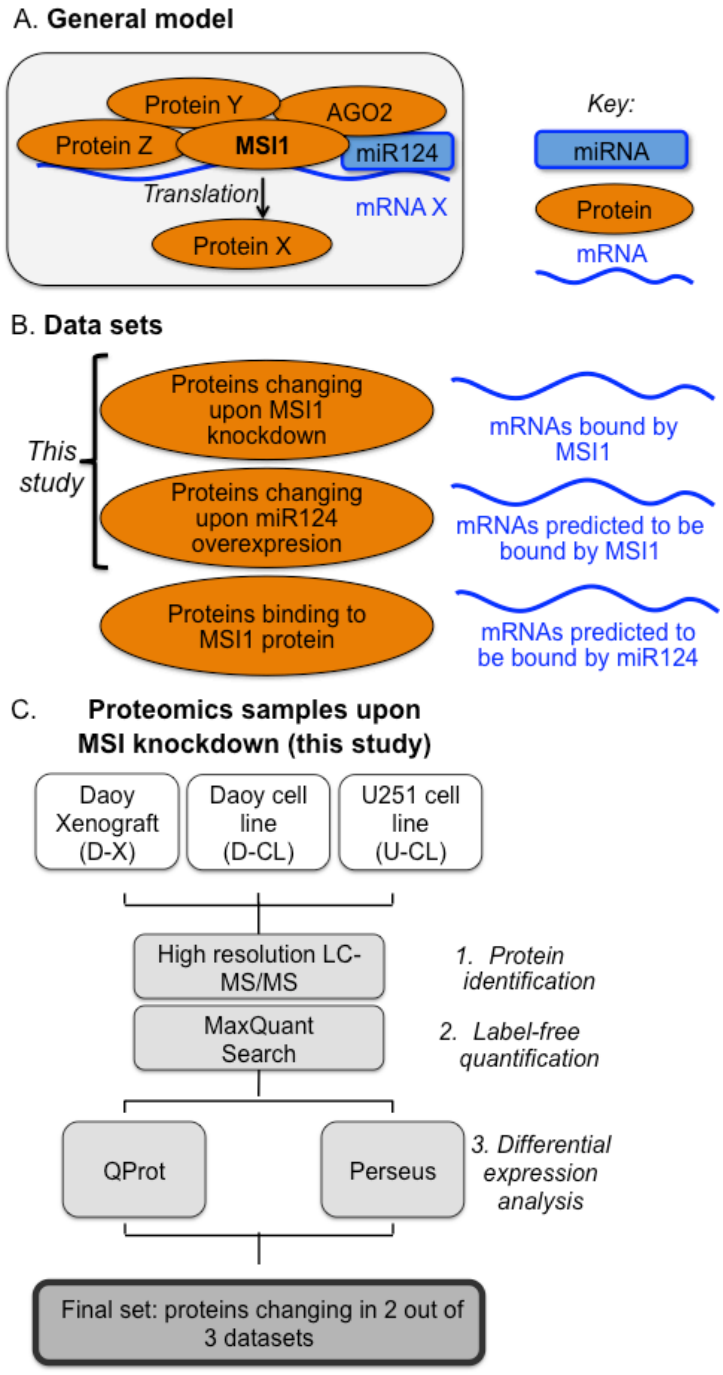

Figure 2: Three proteomics analyses of MSI1 knockdown

A. Quantitative proteome changes upon MSI1 knockdown. Proteins are taken from the intersections of B. and C., requiring significant up- or down-regulation in two of the three independent studies. **B., C**. Intersection of the three different studies of MSI1 knockdown. Up(**B**)- and down(**C**)-regulated proteins were defined as specified in the Methods. D-X : Daoy xenograft, D-CL: Daoy cell line, U-CL: U251 cell line. **D.** Function enrichment (FDR < 5).

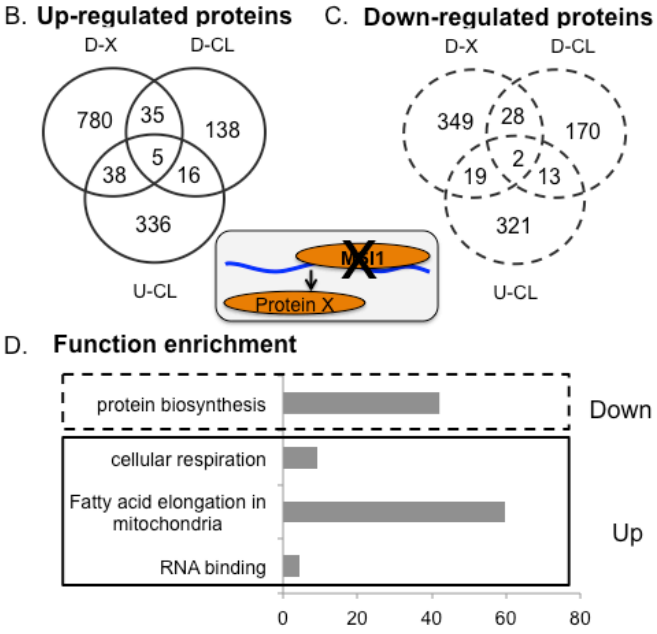

Figure 3. Intersection of complementary datasets suggests a functional relationship between MSI1 and miR124
Datasets collected in-house and from publications were analyzed for significant intersections using hypergeometric tests (see Methods). The total number of proteins in each test was defined as N=2000 for **A, B, C,** and **D**. Up- and down-regulated proteins were identified by proteomics analysis of an MSI1 knockdown (see Methods) and **Figure 2**. Sets in **A, C,** and **D** overlap significantly (p-value<0.05) indicating a functional relationship between MSI1 and miR124. Proteins from the intersection of **A**. and **C**., i.e. PTRF and DHCR24 from panel **D**. were used to test this hypothesis.

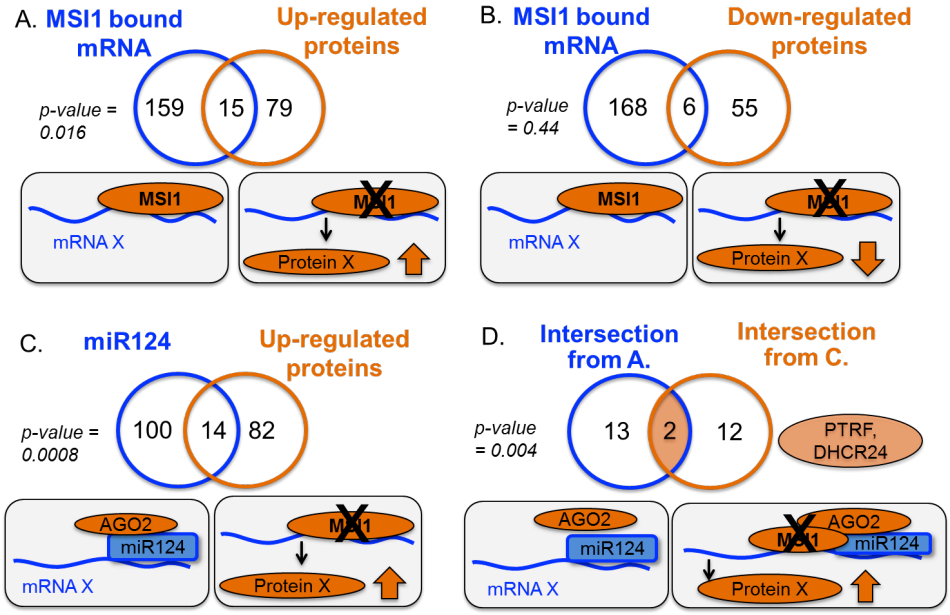

Figure 4. Testing a functional relationship between MSI1 and miR124
If a functional relationship between MSI1 and miR124 exists, we predict that miR124 is up-regulated in cells under MSI1 knockdown, and that MSI1 is down-regulated in cells under miR124 overexpression. **A**. We validated the first hypothesis by qPCR of miR124 in U251 cells in which MSI1 was knocked-down. **B.** We tested the second hypothesis using anti-MSI1 western blotting in U251 cells in which miR124 was overexpressed. We tested three biological replicates for both control and mir124 overexpressed cells. MSI1 does not change expression in miR124 overexpressed cells, but is present in high concentrations in both samples – consistent with a model in which MSI1 impacts miR124 expression, but not *vice versa* (see **Figure 5** and Discussion). PTRF and DHCR24 decrease their expression after overexpressing mir124 confirming the predictions (see **Figure 5,**). We used actin as a loading control. C) LFQ intensities of PTRF, DHCR24 and MSI1.

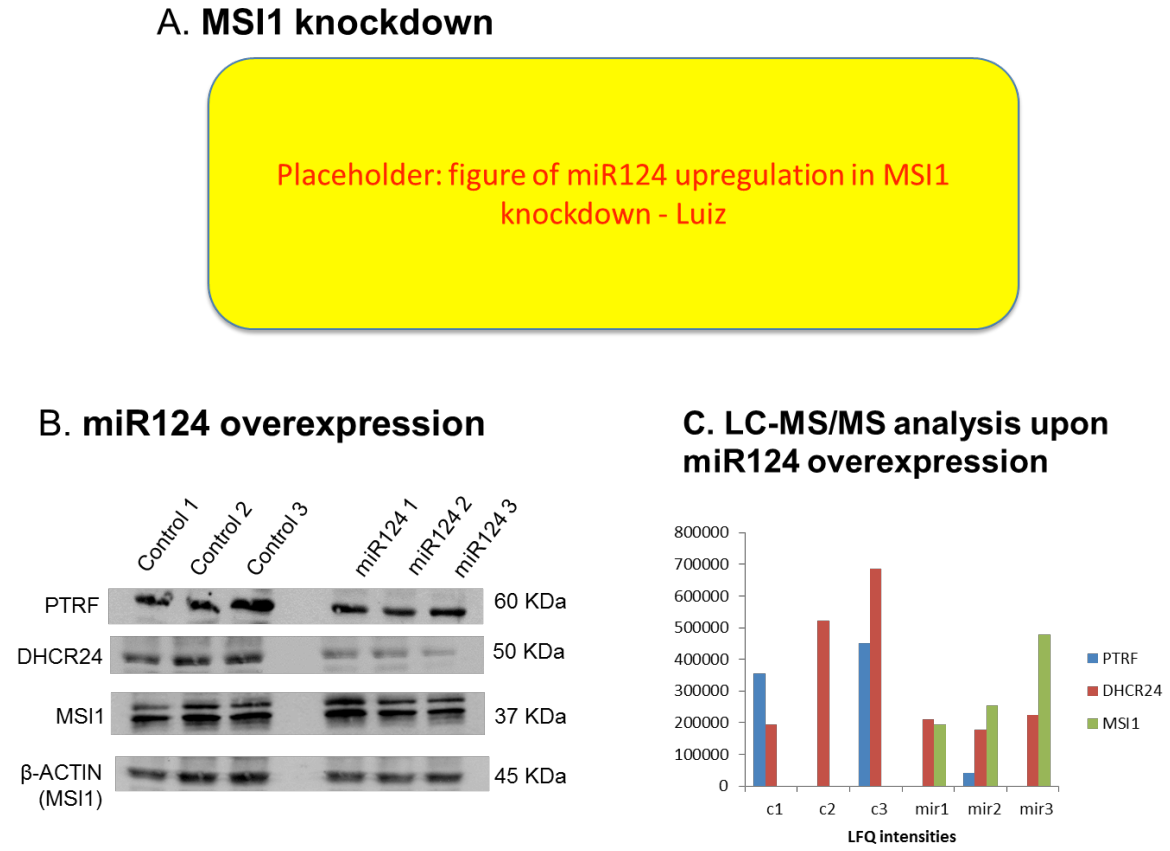

Figure 5. Proteomics analysis of miR124 overexpression confirms a uni-directional relationship
A. Proteomics analysis upon miR124 overexpression. The heatmap shows the normalized LFQ intensities in 3 biological replicates. Blue – proteins downregulated, red – proteins upregulated. **B**. Datasets collected in-house from MSI1 KD and miR124 overexpression were analyzed for significant intersections using hypergeometric tests (see Methods). The total number of proteins in each test was defined as N=2000. Considering miR124 function as a gene repressor, we used only the downregulated proteins for the intersection with MSI1 KD up- and down-regulated proteins.

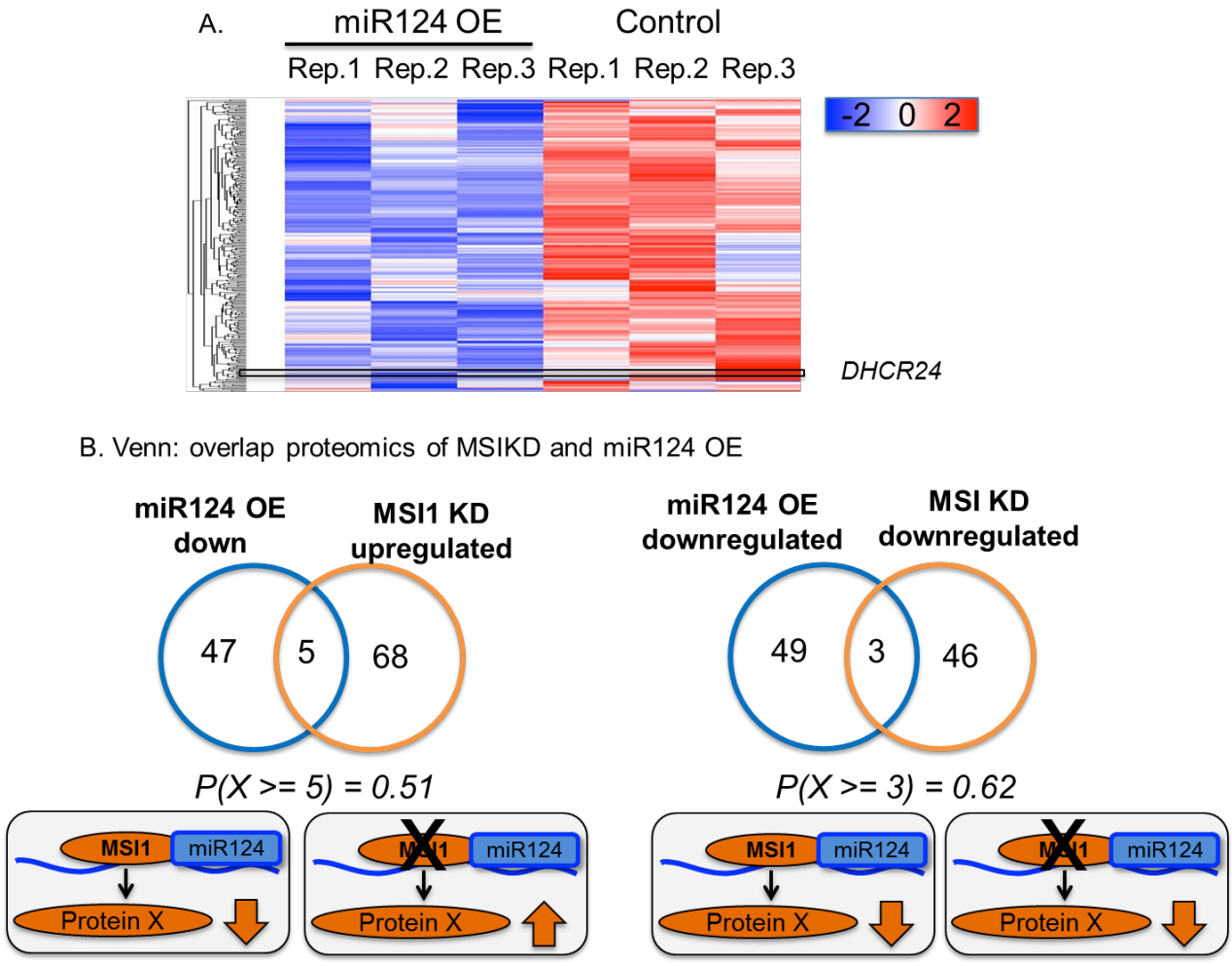

Figure 6. Graphical representation of our model

A. Summary of the effects of MSI1 and miR124 on the expression of DHCR24 and PTRF in normal and brain tumor cells (left) and the MSI1 knockdown and miR124 overexpression experiments (right). MSI1 potentially represses translation of DHCR24 and PTRF, while miR124 does not have an impact. **B**. Model of putative regulatory interactions between MSI1 and miR124 that are consistent with our study. MSI1 positively impacts expression of miR124, either directly or indirectly. Blue - miR124, orange – proteins, blue strand– mRNA, blue rectangle – miR-124. The size of the oval represents relative expression changes. Double lines signify results from this study; dotted lines unknown values. Yellow block arrows signify putative regulatory relationships.

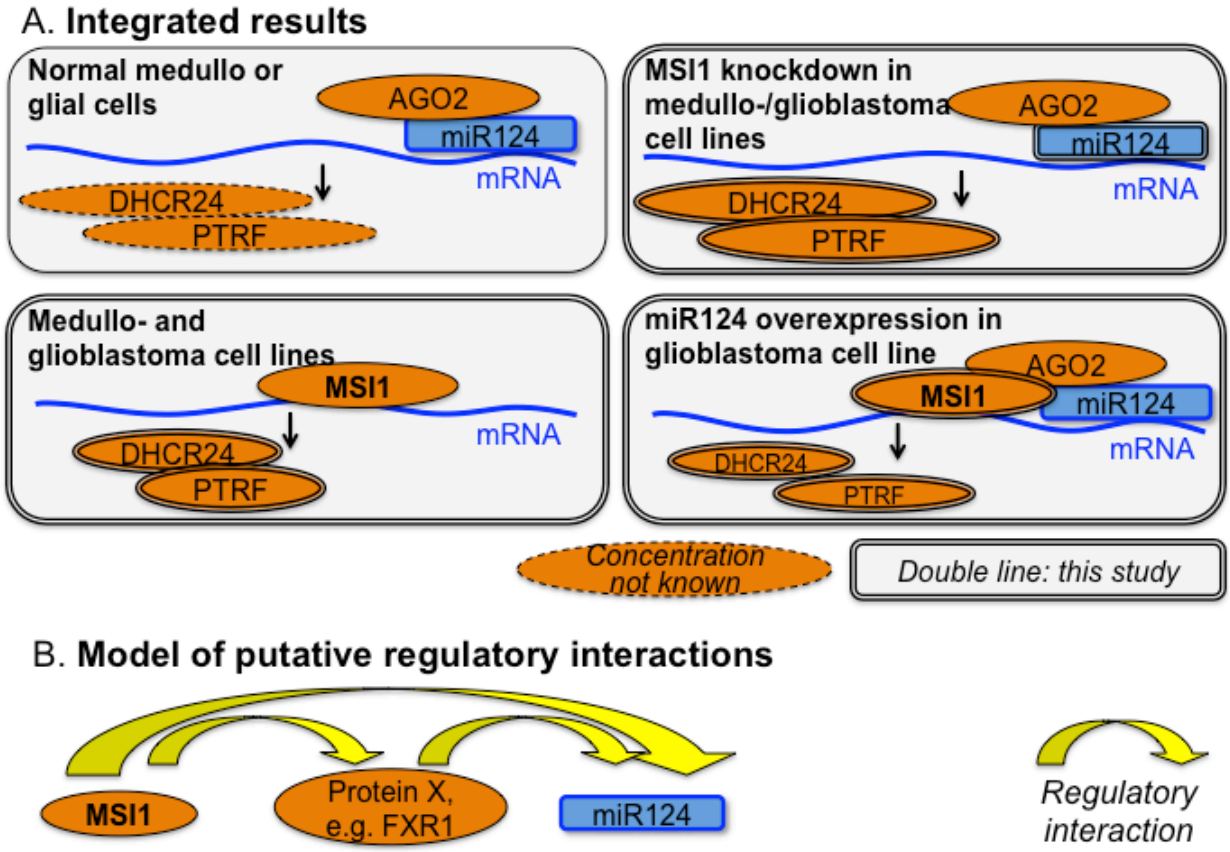

Table 1. Proteins up- or down-regulated in the MSI1 knockdown and mRNA bound by the MSI1 protein
Function annotations were taken from UniprotKB **REF**. The prediction of the MSI1 recognition motif in the 3'UTR of the mRNA was taken from MEME Suite **REF**. The role in cancer formation was estimated based on Uniprot KB and OMIM **REF**, finally the GO annotations were taken from NCBI David Bioinformatics Suite **REF**. Information on the MSI1 protein binding to the mRNA was taken from published experimental studies [30, 61]. miRNA validated target are taken from miRTarBase **REF**. For clarity, only the presence of a feature is marked (with Y), not its absence. The proteins are sorted according to the presence of features. The Supplement has the extended table, see **Table SXXX**. * Protein is differentially expressed in all three MSI1 knockdown datasets.

Gene	Function	Cancer / cell division	Motif in 3'UTR suggesting MSI protein binding	MSI1 protein bound to mRNA	mir12 4-3p	mir18 a-3p
A. Up-regulated proteins						
DHCR24	regulation of neuron death	Y	Y	Y	Y	Y
PTRF	induces senescence	Y		Y	Y	
TBL1XR1	canonical Wnt signaling pathway	Y (leukemia)		Y		
MAP4	cell division	Y		Y		
MTDH	regulation of apoptotic process	Y	Y	Y		
MYOF	regulation of vascular endothelial growth factor receptor signaling	Y	Y	Y		
SSR1	regulation of cell proliferation	Y	Y	Y		
CMTM6	chemotaxis		Y	Y		
FAF2	response to unfolded protein		Y	Y		
IGF2R	insulin-like growth factor receptor signaling pathway		Y	Y		
FLNB	actin cytoskeleton organization			Y		
MAVS	RIG-I signaling pathway			Y		
NUCKS1	RNA binding protein			Y		
PPT1	brain development			Y		
TXNDC5	apoptotic cell clearance			Y		
B. Down-regulated proteins						
CDV3	cell proliferation	Y	Y	Y	Y	
ADD1	apoptotic process	Y	Y	Y		
ANXA1	regulation of apoptotic process	Y		Y	Y	
PKM2	programmed cell death	Y		Y		
RPL28	constituent of ribosome			Y		Y
RPS2	nonsense-mediated decay			Y		Y

Biomolecules **2015**, *5*, 1441-1466; doi:10.3390/biom5031441

OPEN ACCESS

biomolecules

ISSN 2218-273X

www.mdpi.com/journal/biomolecules/

Article

Comprehensive Protein Interactome Analysis of a Key RNA Helicase: Detection of Novel Stress Granule Proteins

Rebecca Bish [1,†], Nerea Cuevas-Polo [1,†], Zhe Cheng [1], Dolores Hambardzumyan [2], Mathias Munschauer [3], Markus Landthaler [3] and Christine Vogel [1,*]

[1] Center for Genomics and Systems Biology, Department of Biology, New York University, 12 Waverly Place, New York, NY 10003, USA; E-Mails: rebeccabish@gmail.com (R.B.); nerea.cuevaspolo@gmail.com (N.C.-P.); zhe.cheng@nyu.edu (Z.C.)

[2] The Cleveland Clinic, Department of Neurosciences, Lerner Research Institute, 9500 Euclid Avenue, Cleveland, OH 44195, USA; E-Mail: hambard@ccf.org

[3] RNA Biology and Post-Transcriptional Regulation, Max-Delbrück-Center for Molecular Medicine, Berlin-Buch, Robert-Rössle-Str. 10, Berlin 13092, Germany; E-Mails: mathias@broadinstitute.org (M.M.); markus.landthaler@mdc-berlin.de (M.L.)

† These authors contributed equally to this work.

* Author to whom correspondence should be addressed; E-Mail: cvogel@nyu.edu; Tel.: +1-212-998-3976; Fax: +1-212-995-4015.

Academic Editor: André P. Gerber

Received: 10 May 2015 / Accepted: 15 June 2015 / Published: 15 July 2015

Abstract: DDX6 (p54/RCK) is a human RNA helicase with central roles in mRNA decay and translation repression. To help our understanding of how DDX6 performs these multiple functions, we conducted the first unbiased, large-scale study to map the DDX6-centric protein-protein interactome using immunoprecipitation and mass spectrometry. Using DDX6 as bait, we identify a high-confidence and high-quality set of protein interaction partners which are enriched for functions in RNA metabolism and ribosomal proteins. The screen is highly specific, maximizing the number of true positives, as demonstrated by the validation of 81% (47/58) of the RNA-independent interactors through known functions and interactions. Importantly, we minimize the number of indirect interaction partners through use of a nuclease-based digestion to eliminate RNA. We describe eleven new interactors, including proteins involved in splicing which is an as-yet unknown role for DDX6. We validated and characterized in more detail the interaction of DDX6 with Nuclear fragile X mental retardation-interacting protein 2 (NUFIP2) and with two previously uncharacterized

proteins, FAM195A and FAM195B (here referred to as granulin-1 and granulin-2, or GRAN1 and GRAN2). We show that NUFIP2, GRAN1, and GRAN2 are not P-body components, but re-localize to stress granules upon exposure to stress, suggesting a function in translation repression in the cellular stress response. Using a complementary analysis that resolved DDX6's multiple complex memberships, we further validated these interaction partners and the presence of splicing factors. As DDX6 also interacts with the E3 SUMO ligase TIF1β, we tested for and observed a significant enrichment of sumoylation amongst DDX6's interaction partners. Our results represent the most comprehensive screen for direct interaction partners of a key regulator of RNA life cycle and localization, highlighting new stress granule components and possible DDX6 functions—many of which are likely conserved across eukaryotes.

Keywords: DDX6; post-transcriptional regulation; protein interactions; SUMOylation; NUFIP2; FAM195A; FAM195B; stress granules; P bodies; mRNA degradation

1. Introduction

The concentrations of cellular proteins are finely tuned by a wide variety of regulatory mechanisms at the level of transcription, translation, and degradation. While transcription regulation is an essential process, some studies indicate that post-transcriptional regulation also plays a large role [1–4], encompassing for example RNA processing, storage, degradation, and translation. Over a thousand human proteins appear to have RNA binding functions and therefore putative roles in post-transcriptional regulation [5]. However, in-depth knowledge of the molecular functions, targets, and binding sites is still limited to only several dozen RNA-binding proteins (RBPs) [5–7]—and an accurate understanding of the regulation of protein expression requires further exploration of the network of post-transcriptional regulators with respect to their localization, interaction partners, and functions.

The mammalian DEAD-box RNA helicase DDX6 (also known as p54/Rck) impacts protein expression in several ways [8–11]. Current research suggests that DDX6 may be involved in several key functions of RNA metabolism, determining determine whether an mRNA is destined for translation, storage, or decay [12–16]. Mechanistic effects of the yeast DDX6 ortholog, Dhh1p, on gene expression have been well studied, with translation being repressed at the initiation phase in a nutrient-responsive manner [16]. Dhh1p also associates with ribosomes, and inhibits mRNA translation concomitant with the elongation step when tethered to the mRNA [17]. With respect to mRNA decapping, DDX6 is important for assembly of the decapping complex [18], and may stimulate DCP2 activity [15]. DDX6-dependent inhibition of protein synthesis (*i.e.*, translation inhibition and mRNA decapping) is thought to converge in the miRNA-silencing pathway, where efficient miRISC-dependent repression requires DDX6 [19]. Thus, while DDX6 is required for miRNA silencing, the precise manner by which DDX6 is recruited to miRNA targets remains poorly understood [20]. DDX6 has also been linked to human disease both as a proto-oncogene in several types of cancer [21–24], and as a facilitator of the infection process by a number of viruses including

HIV and the hepatitis C virus [25–28]. However, the exact mechanisms by which DDX6 contributes to these pathogenic processes are yet to be determined.

Both the sequence and functions of DDX6 are conserved in a variety of organisms including *S. cerevisiae* (DHH1) [29], *S. pombe* (STE13) [30], *C. elegans* (CGH-1) [31], *D. melanogaster* (Me31B) [32], *X. laevis* (XP54) [33], and mammals [34]. DDX6 has a complex localization pattern: it stains diffusely in the nucleus and cytoplasm, and localizes both constitutively and during stress to at least two different mRNA-protein (mRNP) structures in the cytoplasm, *i.e.*, stress granules and P-bodies [35–38]. The multiple niches to which DDX6 localizes likely reflect the multiple molecular mechanisms by which DDX6 influences post-transcriptional gene regulation [39]. In one of these functions, DDX6 enhances mRNA decay via the decapping pathway, a role which has been associated with cytoplasmic structures known as P-bodies or GW bodies [14,35,40]. DDX6 is also involved in the repression of mRNA translation at a step following initiation [16,17,41,42]. Under cellular stress, this translation repressor function has been linked to the storage of mRNAs in cytoplasmic bodies known as stress granules [37]. P-bodies, which are constitutively present in most cell types, have an overlapping but distinct protein composition as compared with stress granules, which are inducibly assembled when global protein synthesis is inhibited in response to stress [43]. Finally, DDX6 can alter protein levels via regulation of microRNA activity [8,9,20,44,45].

Despite much recent investigation [11,13,20,46,47], the mechanisms by which DDX6 carries out these diverse functions are still not well understood. A small number of interactions between DDX6 and other proteins have been characterized in several organisms, but overall the evidence is fragmented and anecdotal. For example, DDX6 is known to interact with the decapping proteins DCP1 and EDC3 in processing bodies (P bodies), forming a complex which mediates de-adenylation dependent mRNA decay [14,35,40,48]. An interaction between DDX6 and the Argonaute proteins, which work in concert with miRNAs to regulate protein levels, has also been posited to occur within P-bodies [44]. DDX6 has further been shown to interact with the translation repressors ataxin-2/ataxin-2 like protein (ATXN2/ATXN2L) and polyadenylate-binding protein 1 (PABPC1) both under normal conditions (where no stress granules are present), and within stress granules under appropriate conditions [37,49].

While these known DDX6 interactions are suggestive of the mechanisms by which DDX6 exerts its influence on post-transcriptional regulation, only a systematic and comprehensive investigation of the protein interaction partners enables us to fully understand the scope and mechanism of DDX6 function. We undertook such an unbiased study of the DDX6-centric protein interactome to shed light on its role in post-transcriptional regulation of cellular protein levels. As a result, we have expanded our knowledge of the proteins involved in DDX6-mediated processes, and identified, verified, and characterized new proteins which re-localize to stress granules under conditions of cellular stress.

2. Results

2.1. Identification of DDX6-Interacting Proteins

To identify proteins which interact with DDX6, we created an HEK293-based cell line which stably expresses DDX6 fused with an N-terminal FLAG/HA-tag under control of a tetracycline-inducible promoter (293-DDX6-FH). Previous reports indicate that high-level overexpression of DDX6 can

induce the formation of additional P bodies, as observed for other P body proteins [16,50]. To avoid this scenario, we selected a clone of the 293-DDX6-FH line which upon induction resulted in expression of DDX6-FLAG-HA at approximately 80% of the level of wild type DDX6 expression (Figure 1A). Repeat experiments demonstrated that this clone reproducibly results in FLAG/HA-DDX6 levels of 70%–90% of endogenous DDX6 levels after 18 h of doxycycline induction. We further confirmed that the DDX6-FLAG-HA protein localizes to P bodies in a manner indistinguishable from that of endogenous DDX6 (Figure 1B), and that the average number of P bodies per cell is unchanged by DDX6-FLAG-HA expression (Figure 1C). These results suggest that the DDX6 transgene is fully functional in terms of localization, and does not alter cellular mRNP composition.

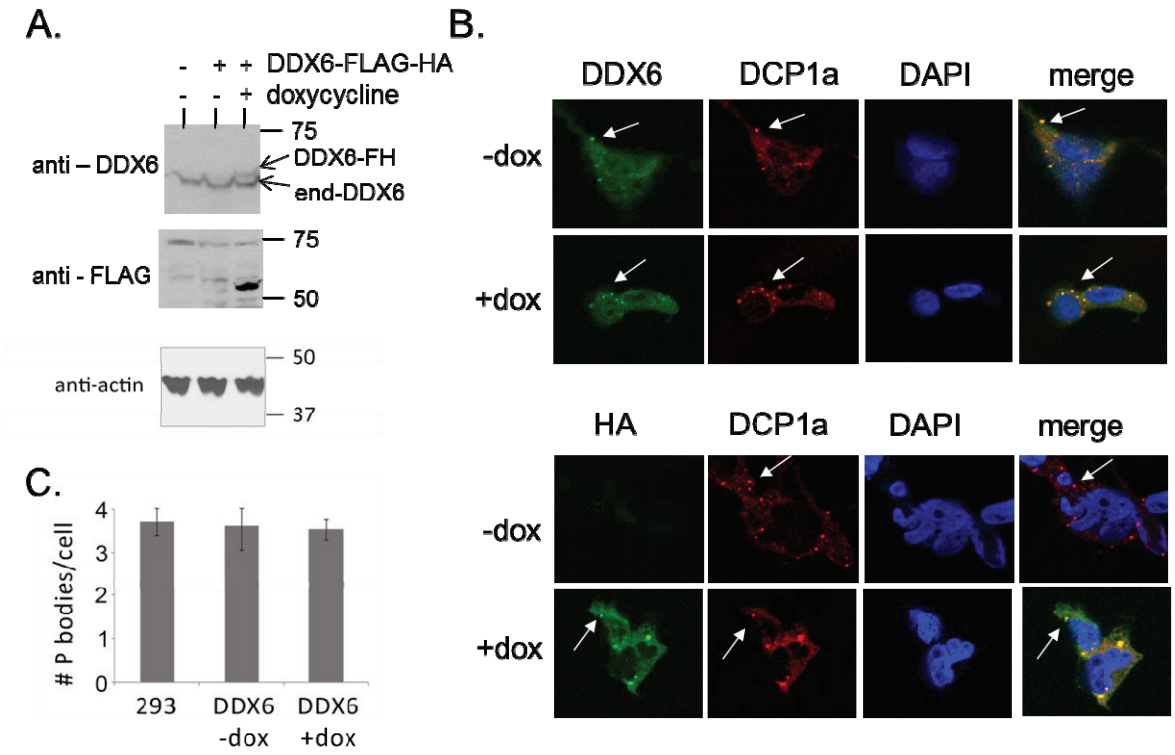

Figure 1. Validation of double-tagged DDX6 construct to ensure highly specific interaction screen. (**A**) Exogenously expressed DDX6 has physiological expression levels. Western blot analysis of whole cell lysates from HEK-293 cells (lane 1) or HEK-293 cells containing the DDX6-FLAG-HA construct under control of a tetracycline-inducible promoter (lanes 2 and 3). DDX6-FH = FLAG-HA-tagged DDX6 construct inducibly expressed from 293-DDX6-FH cells. End-DDX6 = endogenous DDX6; (**B**) Exogenously expressed DDX6 localizes to the expected cellular compartments. Immunofluorescence analysis of HEK-293-DDX6-FLAG-HA cells, in the absence or presence of doxycycline, with antibodies against endogenous DDX6 or the HA epitope tag; (**C**) Quantification of the average number of P bodies per cell in HEK-293 cells as compared to 293-DDX6-FH cells in the absence or presence of doxycycline.

We employed two major approaches to characterize both the direct and indirect interaction partners for DDX6 (Figure 2A). First, we used the double-tagged DDX6 protein as bait in a tandem-pulldown experiment which, due to the two consecutive purification steps is likely to be enriched in true-positive

interaction partners. To do so, we harvested whole cell lysate from 293-FLAG-HA cells treated with doxycycline, and performed a tandem immunoprecipitation (IP) against the FLAG and HA epitope tags. RNA-dependent interactions, *i.e.*, proteins bound to the same RNA but not to DDX6, were removed by benzoase treatment, a highly active nuclease which nonspecifically degrades both RNA and DNA. Identical experiments performed in doxycycline-treated HEK293 cells lacking the DDX6-FLAG-HA construct served as a control for non-specific binding. The purified proteins were digested with trypsin and the resulting peptides were identified by mass spectrometry. Second, in a complementary approach, we used single-pulldown of DDX6 and native-gel electrophoresis to separate different protein complexes involving DDX6. Importantly, our protocol involves a benzoase digestion step which removes all RNA. Therefore, in contrast to many other studies, e.g., [51], our results report very few false-positive interaction partners, *i.e.*, proteins that are purely reported due to their binding to the same RNA.

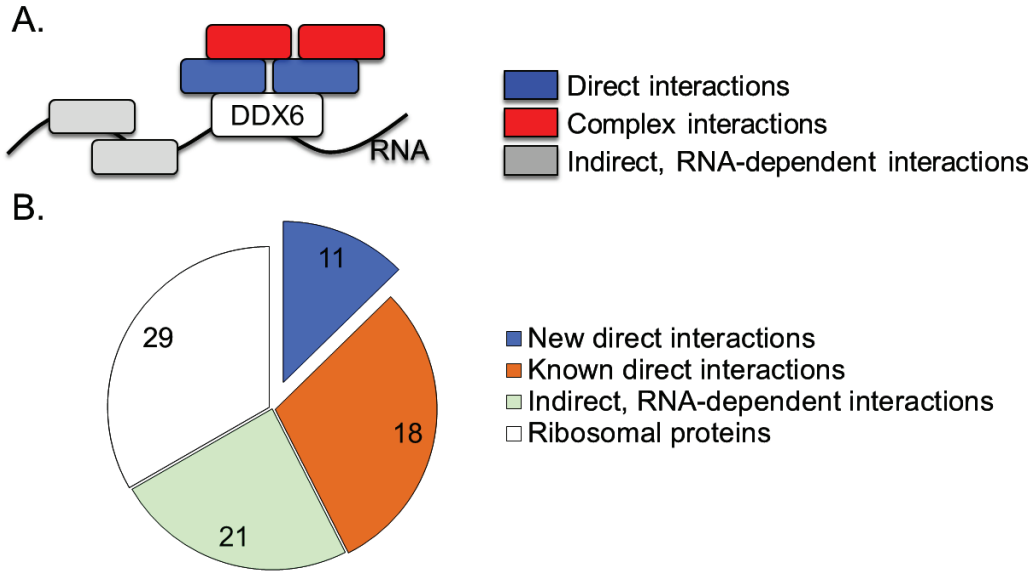

Figure 2. DDX6-interacting proteins belong to three major categories. (**A**) Graphical representation of interaction types identified in this screen. Blue—direct interactions, enriched in pulldown of double-tagged DDX6. Red—complex interactions, identified in native gel experiment. Grey—RNA-dependent interactions; (**B**) DDX6-interacting proteins identified in this screen. The novel, non-ribosomal proteins, likely to be direct interaction partners, are emphasized in blue. Each pie wedge is labeled with the number of proteins identified in that category.

Several criteria were applied to ensure the validity of the list of DDX6-interacting proteins. We applied a 5% false discovery rate cutoff to each individual replicate, and included only proteins which were identified by at least one peptide in a minimum of two biological replicates of one experimental condition (control HEK293 *vs.* experimental 293-DDX6-FH IP) on the list. Furthermore, any protein identified by a single peptide in the control IP was considered a contaminant and excluded from the list, as were all keratins, histones, and immunoglobins. These strict criteria ensure high confidence in the identified proteins.

Applying these criteria, a total of 81 proteins were identified in the tandem-pulldown experiment, including DDX6 itself (Supplementary data). We subdivided the list into several categories (Figure 2B). As could be expected, we identified more RNA-dependent than independent interactions (Supplementary data). The 23 RNA-dependent proteins are enriched in RNA-binding functions (GO: 0003723), and likely identified due to binding of a common RNA molecule, without maintaining a direct protein-protein interaction. In agreement with this interpretation, none of the RNA-dependent DDX6 interactors had previously been identified as directly binding to DDX6.

A second group of proteins identified as interacting with DDX6 is composed of ribosomal proteins from both the large and small ribosomal subunits (Supplementary data and Figure 2B). A physical interaction between DDX6 and the ribosome is not surprising, given the previously documented interaction of the yeast ortholog DHH1 with the ribosome [17], and the documented role of DDX6 in the regulation of translation efficiency [16,17]. In the interest of focusing on previously uncharacterized DDX6 protein partners, interactions with the ribosome will not be further discussed here.

We identified 29 non-ribosomal proteins as interacting with DDX6, independent of RNA presence, and these proteins represent a core which we examined in more detail (Table 1 and Figure 2B). Amongst the proteins, several functional categories were significantly enriched: RNA binding ($p = 4.7 \times 10^{-8}$), deadenylation-dependent mRNA decay and P-bodies ($p = 2.2 \times 10^{-7}$), and cytoplasmic stress granules ($p = 3.2 \times 10^{-7}$). These categories are in accordance with the known functions of DDX6 in mRNA decay, and its localization to cytoplasmic stress granules [52]. There is a high degree of interconnectivity within the DDX6 interactome, as 25 of the 29 DDX6-interacting proteins identified in this study have been shown to bind at least one other protein within this group (Supplementary data).

A literature search reveals that 18 of the proteins have previously been shown to interact with DDX6: the ATXN2/ATXN2L-PABPC1 complex, the DCP1-EDC3-PAT1L decapping complex, LSM14A, transcription intermediary factor 1-beta (TIF1B), and eukaryotic translation initiation factor 4E transporter (EIF4ENIF1), FAM195A and FAM195B [37,40,48,49,52–54]. For several other proteins, *i.e.*, LSM14B, EDC3, NUFIP2, other large-scale screens reported possible complex or indirect interactions (Table 1). Other proteins are known to be components of stress granules, P-bodies, or the decapping complex which are all functions that are known to involve DDX6 (Table 1). These known interactions and functions to verify that our interaction screen is highly specific.

In total, eleven (19%) of the identified proteins represent novel interactions with DDX6 in the context of human cells that have the potential to provide insight into DDX6-mediated cellular processes (Table 1). Six of these new interactors, namely C1QBP, DDX17, HNRNPC, HNRNPM, RTCB, and THRAP3, are annotated as splicing factors—a function that DDX6 has not previously been implicated in.

Table 1. Interaction partners, independent of binding to RNA.

Gene Name	Protein Name	SG	TL	PB	DC	Status	SF
ATXN2	ataxin 2	X	X	X		BG	X
ATXN2L	ataxin 2-like	X		X		BG	X
C1QBP	complement component 1, q subcomponent binding protein					New	X
DCP1B	DCP1 decapping enzyme homolog B			X	X	BG	
DDX1	DEAD (Asp-Glu-Ala-Asp) box helicase 1	X	X			Inf	X
DDX17	DEAD (Asp-Glu-Ala-Asp) box helicase 17					New	X
EDC3	enhancer of mRNA decapping 3 homolog			X	X	BG	
EDC4	enhancer of mRNA decapping 4			X	X	BG	
EIF4ENIF1	eukaryotic translation initiation factor 4E nuclear import factor 1					BG	
ERH	enhancer of rudimentary homolog (Drosophila)					New	
FMR1	fragile X mental retardation 1	X	X			New	
FXR2	fragile X mental retardation, autosomal homolog 2		X			New	
G3BP2	GTPase activating protein (SH3 domain) binding protein 2	X				BG	
GRAN1/ FAM195A	family with sequence similarity 195, member A	X***				BG	
GRAN2/ FAM195B	family with sequence similarity 195, member B	X***				BG	
HNRNPC	heterogeneous nuclear ribonucleoprotein C (C1/C2)					New	X
HNRNPM	heterogeneous nuclear ribonucleoprotein M					New	X
LARP4	La ribonucleoprotein domain family, member 4					New	
LSM12	LSM12 homolog					BG	
LSM14A	LSM14A, SCD6 homolog A	X	X	X		BG	
LSM14B	LSM14B, SCD6 homolog B		X			BG	X
NUFIP2	nuclear fragile X mental retardation protein interacting protein 2	X***				BG	
PABPC1	poly(A) binding protein, cytoplasmic 1	X	X			Inf	X
PABPC3	poly(A) binding protein, cytoplasmic 3	X				Inf	
PABPC4	poly(A) binding protein, cytoplasmic 4 (inducible form)	X	X			Inf	X
PATL1	protein associated with topoisomerase II homolog 1			X	X	BG	
RTCB	RNA 2',3'-cyclic phosphate and 5'-OH ligase					New	X
THRAP3	thyroid hormone receptor associated protein 3					New	X
TIF1B	tripartite motif containing 28					New	

Proteins identified by mass spectrometry from samples generated by immunoprecipitation of DDX6 from nuclease-treated samples. Status—status of interaction (New—interaction partner newly detected in this screen; Inf—interaction can be inferred from DDX6's new function in DC, SG, TL, or PB; BG—interaction with DDX6 reported in Biogrid [55]). SG—stress granules. TL—translation. PB—processing bodies. DC—decapping complex. SF—splicing factor. ***—as demonstrated in this paper.

2.2. Validation and Characterization of Direct Interactions with NUFIP2, GRAN1 (FAM195A), and GRAN2 (FAM195B)

We chose three of the DDX6-interacting proteins for further validation and characterization as very little or nothing was known about their function: NUFIP2, FAM195A, and FAM195B. FAM195A and FAM195B have recently been listed as DDX6 interaction partners in a large-scale experiment [53], but this result has not yet been validated or characterized. Due to results that will be discussed below, we have renamed the genes as granulin-1 (GRAN1, FAM195A) and granulin-2 (GRAN2, FAM195B). NUFIP2 has also not been well-characterized, but has been shown to associate with Fragile X Mental Retardation Protein (FMR1, also identified as DDX6-interacting protein in this study) and the polysome [56,57]. First, to confirm the interactions with DDX6, we performed an immunoprecipitation using anti-FLAG antibodies in lysate prepared from 293-DDX6-FH cells, and subjected the purified proteins to Western blot with antibodies specific to NUFIP2, GRAN1, and GRAN2 (Figure 3A). For all three antibodies, a band was identified at the correct molecular weight in whole cell lysates. A similar band was observed when blotting proteins purified specifically in the IPs from 293-DDX6-FH cells but not the control HEK-293 cells, validating the interactions observed by mass spectrometry.

We then examined the co-localization of NUFIP2, GRAN1, and GRAN2 with DDX6 by performing immunofluorescence experiments in HEK-293 cells with antibodies specific to each protein. All three proteins showed dual localization to the cytoplasm and nucleus, and they exhibit diffuse staining both in the nucleus and cytoplasm which overlap with the diffuse DDX6 staining (Figure 3B). However, none of the three proteins stain within P bodies, as can be seen by the lack of co-localization in the DDX6-positive cytoplasmic foci (Figure 3B).

GRAN1 and GRAN2 are small proteins distinguished primarily by the presence of the FAM195 protein domain (Figure 4A). They have not yet been described in literature. Mass spectrometry data indicates that both GRAN1 and GRAN2 possess a similar cluster of phosphorylation sites in the N-terminal side of the FAM195 domain (Figure 4A) [58]. GRAN1 and GRAN2 protein levels appear to be influenced by DDX6 expression, as induction of DDX6 overexpression in 293-DDX6-FH cells by doxycycline treatment induced a significant increase in GRAN1 and GRAN2 levels compared to the loading control of beta-actin, as measured by Western blotting of whole cell lysates (Figure 4B). This increase in GRAN1 and GRAN2 expression could happen through a number of different mechanisms, including translational regulation or stabilization of GRAN1 and GRAN2 protein levels via complex formation with DDX6.

Next, because of their similar localization patterns, we tested whether GRAN1 and GRAN2 interact by immunoprecipitating GRAN2 from HEK293 cells and blotting for GRAN1 and DDX6 (Figure 4C). This experiment indicates that GRAN1 and GRAN2 do interact, and also confirms the DDX6 interaction via a reciprocal co-immunoprecipitation.

We next examined the subcellular localization pattern of GRAN1, GRAN2, and NUFIP2, to gain additional insight into their potential functions. DDX6 undergoes a change in subcellular localization after exposure of cells to various types of stress that induce the formation of stress granules [37,38]. DDX6 can still be found in P bodies under these conditions, but some fraction of DDX6 protein also re-localizes to stress granules. We hypothesized that, since NUFIP2, GRAN1, and GRAN2 are not found in P bodies, they might instead localize to stress granules under the appropriate conditions. This

hypothesis is strengthened by the observation that both NUFIP2 and GRAN1 contain Q/N-rich regions (Figure 4A) which have been shown in other proteins to mediate localization to cytoplasmic mRNP particles such as stress granules [59]. Furthermore, NUFIP2 precipitates from cells after treatment with biotinylated 5-aryl-isoxazole-3-carboxyamide, a compound which induces the precipitation of many RNA binding proteins which are constituents of mRNP granules [60].

To test the hypothesis that GRAN1, GRAN2, and NUFIP2 might localize to other mRNP granules, we treated HEK293 cells with arsenite, a reagent known to induce stress granules. We then performed double-immunofluorescence imaging to co-localize these proteins with PABPC1, a well-characterized marker of stress granules (Figure 4D). GRAN1, GRAN2, and NUFIP2 all exhibited a dramatic change in sub-cellular localization upon arsenite treatment, forming cytoplasmic foci that perfectly overlap with stress granules (Figure 4D). These data, combined with their interaction with DDX6, suggests a role for these three proteins in granule formation after stress.

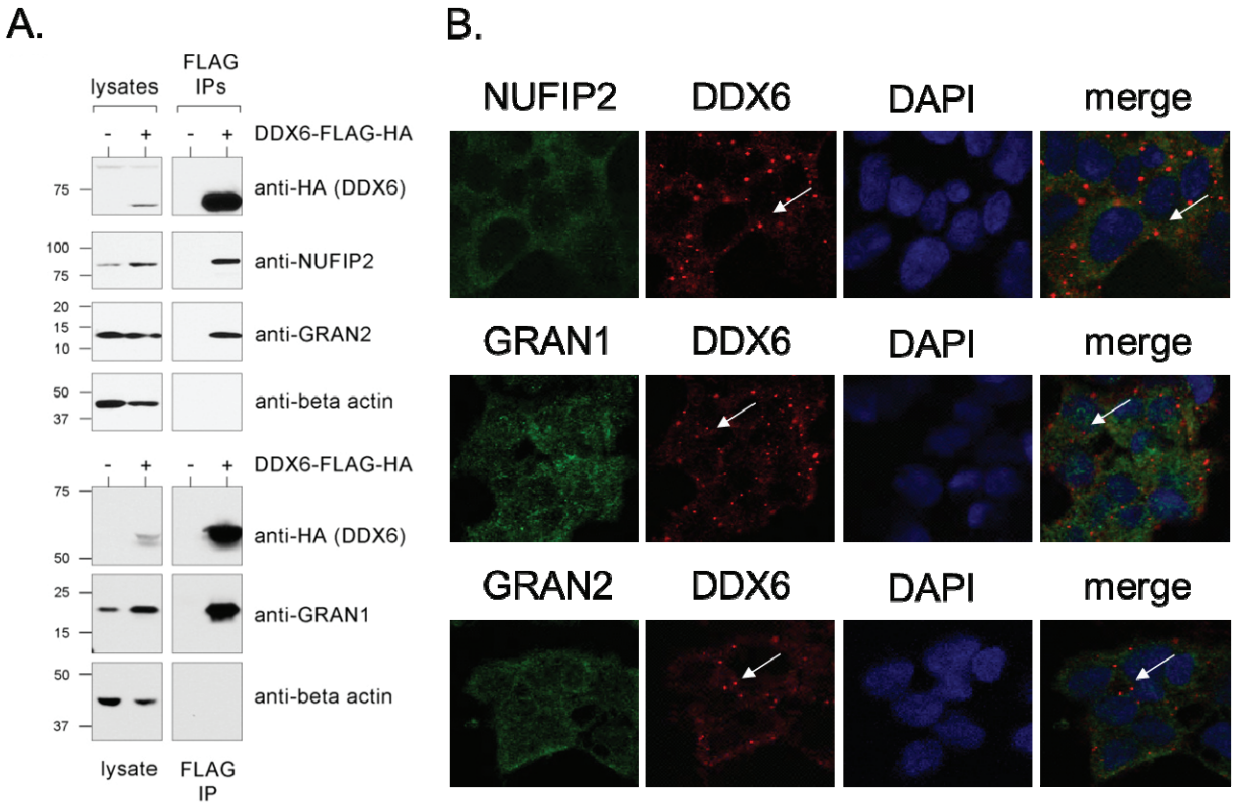

Figure 3. Validation of direct interactions—characterization of new genes. (**A**) DDX6 interacts with NUFIP2, GRAN1, and GRAN2. Whole cell lysate (lanes 1 and 2) or tandem FLAG/HA immunoprecipitates (lanes 3 and 4) were probed by Western blot with antibodies against the HA epitope tag, NUFIP2, GRAN1, GRAN2 or beta-actin (loading control). The experiment was performed in HEK-293 cells (control) or in 293-DDX6-FH cells induced with doxycycline as indicated; (**B**) NUFIP2, GRAN1, and GRAN2 do not localize to P bodies. For the co-localization of DDX6 with GRAN1, GRAN2, and NUFIP2, cells were double-stained with an antibody against DDX6 (red) and the interacting proteins as indicated (green). Nuclei are marked with DAPI. White arrows indicate the location of a DDX6-positive P body.

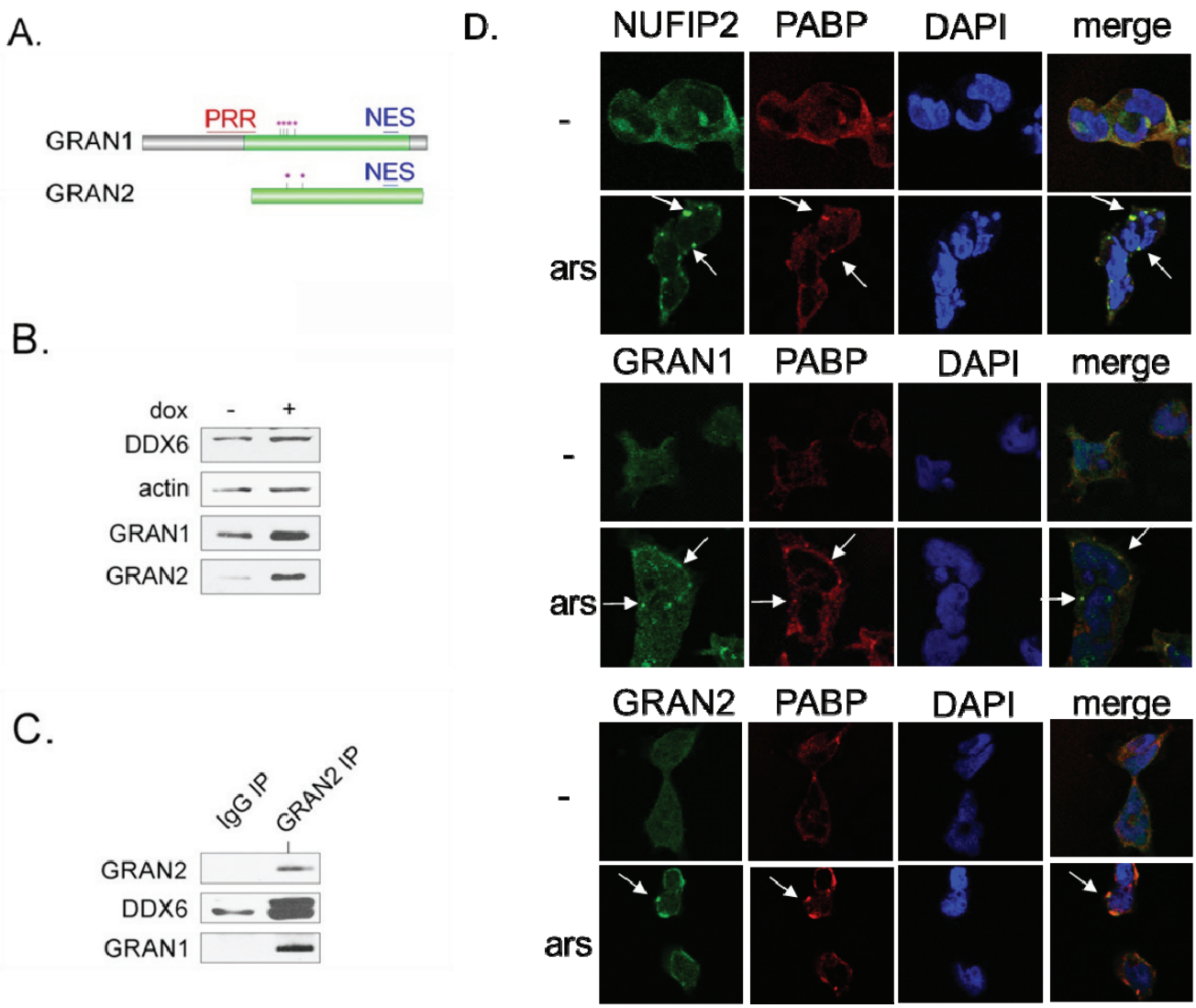

Figure 4. GRAN1, GRAN2, and NUFIP2 localize to stress granules upon arsenite treatment. (**A**) Domain structure and features of GRAN1 (FAM195A) and GRAN2 (FAM195B). Green = FAM195 domain [61]. PRR = proline-rich region. NES = nuclear export signal [62,63]. Purple stars = serine/threonine phosphorylation sites from the PhosphoSite database [58]; (**B**) GRAN1 and GRAN2 protein levels increase upon induction of DDX6 overexpression. Whole cell lysates from 293-DDX6-FH in the absence or presence of doxycycline were separated by SDS-PAGE and blotted with the indicated antibodies; (**C**) GRAN1 and GRAN2 form a physical complex. An immunoprecipitation experiment with an anti-GRAN2 antibody was subject Western blot with antibodies that recognize GRAN2 and DDX6; (**D**) NUFIP2, GRAN1, and GRAN2 localize to stress granules. HEK293 cells were either mock-treated (-) or subject to arsenite (ars) treatment (50 mM, 1 h) prior to immunofluorescence staining with antibodies against NUFIP2, GRAN1, or GRAN2. Stress granules were identified by staining with the stress granule marker PAPB, and DAPI marks the location of the nucleus. White arrows indicate stress granules.

2.3. Further Functional Characterization of the DDX6 Interactome

Based on the data discussed above (Table 1) and literature evidence, we hypothesized that DDX6 belongs to several distinct multi-protein complexes, playing a role in different aspects of RNA metabolism (e.g., decapping, splicing, translation regulation, transport), is localized to different cellular compartments (e.g., P bodies, stress granules, diffuse cytoplasmic and nuclear staining). To test this hypothesis, we purified DDX6-protein complexes by immunoprecipitation from 293-DDX6-FH cells, and separated the intact protein complexes by blue native polyacrylamide gel electrophoresis [64–66]. The gel lanes from control (HEK293) or 293-DDX6-FH samples were cut into thirty 2 mm slices, and the protein contents were analyzed by mass spectrometry. Identified proteins were classified as either P-body, stress granule, or splicing factors (Figure 5A,B).

We then plotted the number of unique peptides identified in each group according to the gel region which roughly corresponds to the molecular weight of the intact protein complex. Proteins with ambiguous group membership were excluded. In this graph, we note a single peak of splicing factors in the lower molecular weight region (corresponding to approximately 150–300 kD), accompanied by elution of the ribosomal proteins (Figure 5A,B). Notably, elution of splicing proteins is dominated by C1QBP, a protein involved in regulation of RNA splicing by inhibiting the RNA-binding capacity of SRSF1 and its phosphorylation [67]. Is required for the nuclear translocation of splicing factor U2AF1L4 [67]. An interaction with DDX6 has not yet been described.

In the middle molecular weight regions, only the P body proteins are present. In addition, at high molecular weights, both P body and stress granule proteins form an overlapping peak (Figure 5A,B). The co-elution of P-body and stress granule components illustrates the overlapping functionalities and protein membership of these protein complexes. The elution of NUFIP2, GRAN1, and GRAN2 with other known members of stress granules confirms our findings from above on these proteins being new stress granule components (Figure 5B). The separation of protein complexes by molecular weight according to function suggests that DDX6 likely functions in a number of different protein complexes with different functions.

One of the novel DDX6-interacting proteins, TIF1β (Table 1), has recently been identified as an E3 ligase for the small ubiquitin-like protein SUMO [68,69]. Indeed, in one high-throughput study that used mass spectrometry to identify SUMO-conjugated proteins, DDX6 is identified as a sumoylation substrate [70]. We therefore set out to confirm whether DDX6 is sumoylated. We purified DDX6 from 293-DDX6-FH cells by immunoprecipitation, and blotted with an antibody against SUMO1. We observed a band at approximately 65 kD (Figure 5C), leading to the conclusion that DDX6 is sumoylated.

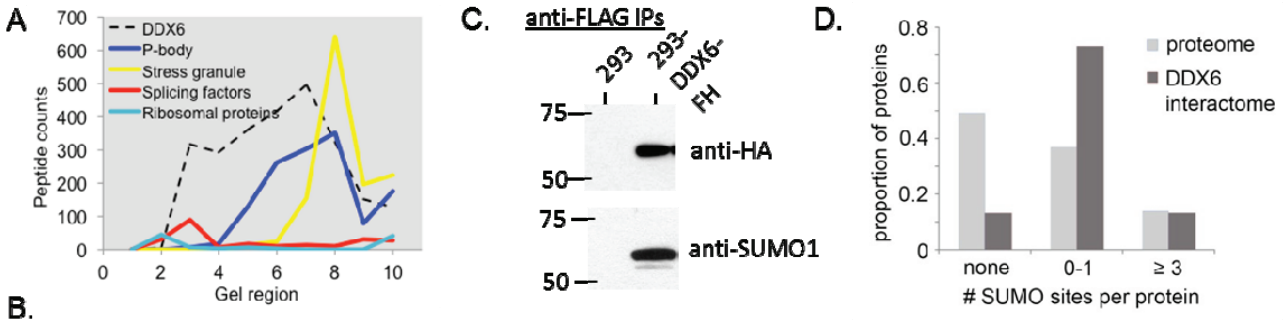

B.

Name	5	6	7	8	9	10	11	12	13	14	15	16	17	18	19	20	21	22	23	24	25	26	27	28	29	30	FB	SG	SF
DDX6	3	3		7	311	195	46	53	69	119	175	104	119	194	181	166	149	146	164	14	56	51	43	46	43	39	x	x	
PATL1											1		1	6	3	3	3	2	4								x	x	
YBX1					13	15	1	5	2	2	3	9	4	17	8	5	3	2	1								x		x
LSM2					1								1	3	1												x		x
DCP1B															1	12	13	19	70	23	4	5	1				x		
EDC3										23	17	9	31	114	104	62	39	47	68	39	10	22	7	11	9	7	x		
EDC4																							1	51	41	16	x		
LSM12	1											3	2	3	4	12	17	19	22	11	6	10	12	9	15	17	x		
LSM14A						8	2			2	37	18	11	19	9	5	5	12	9	1					1		x		
LSM14B				8		8				23	27	14	19	19		12	9		10								x		
PABPC1													3	15	6	8	29	45	48	4	24	45	29	2	53	36		x	x
HNRNPA1	3	2																										x	x
ATXN2																38	62	54	58	42		35	33	44	50	41		x	
ATXN2L																		83	123	74			30					x	
EIF4ENIF1														1	2	1	5	4	4	3		2			3	1		x	
FXR2									7	7		1		3			1	3										x	
G3BP1													10	4			1	1										x	
G3BP2														5	5	1	7	3	5									x	
PABPC3														1		2	2	2	1	1	2	1	1		1	1		x	
PABPC4																2				6		10						x	
NUFIP2																1	4	25	68	46	31	20	18	19	24	20			
GRAN1															1	7	9	8	10	5		6	8	6	5	6		x	
GRAN2																	4	7	4						1			x	
C1QBP	8	12		52	9	1			2	1				4															x
DDX5																										3			x
DHX9										9	1		1		1														x
HNRNPA2B1	3	1																											x
HNRNPA3		4																											x
HNRNPH1				6																			1	2		1			x
HNRNPH2																									6	7			x
IVNS1ABP					5						1	3																	x
PRPF31						4																							x
RBMX				3																									x
SRRM2																					12	11	7	1	5	4			x
SRSF1	3																												x
SNRPD3				7	6	2		1	1	2	1			1	2	3	5	4	2										x
SFPQ														1	1		1	1	2										x

Figure 5. Functional characterization of the DDX6 interactome—complex interactions and SUMOylation. (**A**) Analysis of DDX6-protein complexes by native gel electrophoresis shows that the different functional groupings of DDX6-interacting proteins migrate at different rates, indicating the possibility of distinct DDX6 complexes with different cellular functions. Gel regions represent the combined results from three adjacent gel slices. Proteins with known exclusive membership to a functional class localization (SF—Splicing Factor, PB—Processing bodies, SG—Stress Granules) were grouped and unique peptide counts totaled for the group; (**B**) Distribution of proteins across slices from native gel electrophoresis. We report the number of peptides found for each protein in each slice and their localization. Functional categories as in (A). Highlighted in blue are NUFIP2, GRAN1, and GRAN2 which are further validated and characterized here. The complete dataset is shown in the Supplementary data; (**C**) DDX6 was immunoprecipitated from HEK293 or 293-DDX6-FH cells via a tandem FLAG-HA immunoprecipitation, separated by SDS-PAGE, and blotted with antibodies against SUMO1 and the HA tag to identify sumoylated forms of DDX6; (**D**) DDX6-interacting proteins are significantly enriched in the number of sumoylation sites per protein (t-test, $p = 4.1 \times 10^{-5}$).

We then hypothesized that other members of the DDX6 interactome might be similarly sumoylated. A recent study lead by Mann's group and many other studies that use proteomic approaches to identify sumoylated proteins independently concluded that the identified SUMO-conjugated proteins are highly enriched for proteins involved in RNA metabolism and RNA binding [70–79]. To test whether DDX6-interacting proteins are enriched for sumoylation, we compiled a database of human proteins which have been identified as sumoylated from 14 high-throughput mass spectrometry studies [70–74,77,80–87] (Supplementary data). We included a diverse array of studies, including purifications of SUMO1, SUMO2, and SUMO3, as well as varied purification techniques and experiments performed under stress conditions such as heat shock or oxidative stress, to obtain as wide a representation of the sumoylated universe as possible. In total, 1892 proteins from these studies could be mapped to unique gene identifiers. Of these proteins, 853 were identified by at least two independent studies, and therefore should be considered a core set with especially strong evidence of sumoylation. Of the 29 proteins that we identified as interacting with DDX6 (Table 1), 13 were found to be members of this core set of sumoylated proteins, representing a highly significant enrichment in comparison to the human proteome (hypergeometric test, $p = 3.4 \times 10^{-11}$) (Figure 5C). This enrichment remains significant even when considering the set of all proteins detected in sumoylation studies instead of the entire proteome (19 of 29, $p = 5.6 \times 10^{-9}$). In fact, one of the interactors, heterogeneous nuclear ribonucleoprotein M (HNRNPM), is one of the two most frequently-identified sumoylated proteins known, occurring as a hit in ten of the 14 studies examined (Supplementary data). Conversely, analysis of the human proteome with SUMOsp software to identify high confidence sumoylation sites (both Ψ-K-x-E motif and non-consensus sites) found that the DDX6-interacting proteins identified in this paper contain significantly more sites than would be expected given their frequency in the proteome as a whole (Figure 5D, $p = 4.1 \times 10^{-5}$).

3. Discussion

An extensive body of literature documents the participation of DDX6 in a number of cellular processes, all of which contribute to post-transcriptional regulation and many of which are conserved throughout evolution [16,88,89]. However, the mechanisms by which a protein can act as a regulator are mostly based on interactions with other molecules. To help our understanding of the complex regulatory roles of DDX6, we have undertaken the first comprehensive DDX6-centric interaction screen, and characterized the protein interaction partners in a large-scale, comprehensive manner. To accurately and sensitively identify these proteins, we chose a tandem affinity purification strategy of DDX6 as the bait, coupled to high-resolution mass spectrometry. By combining different approaches, we distinguished functionally relevant interactions with DDX6 from interactions which depend on the mutual binding of RNA, and protein complex membership.

DDX6 is often thought of as a marker of P-bodies [90], and the most well-characterized function of both DDX6 and its yeast ortholog DHH1 is in the mRNA decapping/decay pathway [14,47,88,89,91]. Consistent with this view, we identified a number of P-body/decapping proteins as DDX6 interactors (Table 1). Many of these interactions had previously been observed either in human or yeast in individual studies emphasizing the conservation of DDX6's role across organisms [20,37,46,49,62]. We also identified a number of known and novel interacting proteins which localize to stress granules. Because

these experiments were performed under non-stressed conditions in which stress granules are not visible by microscopy, we conclude that DDX6 maintains stable interactions with stress granule proteins even in the absence of visible mRNP structures. Overall, the sheer number of P-body and stress granule proteins with which DDX6 interacts, in addition to the known mRNP remodeling function of DDX6, suggests that DDX6 may be a key factor in modulating the contents of P bodies and stress granules. Indeed, a recent publication [92] demonstrates a key role of DDX6 in P-body assembly.

Notably, we did not identify any peptides from Argonaute proteins, even below the threshold for inclusion in our lists, despite evidence in the literature that such an Ago-DDX6 interaction does occur [44]. This finding is likely due to either the interaction being transient and not stable enough to persist during the tandem immunoprecipitation protocol, or the interaction taking place under conditions not tested here, or the interaction occurring at a level undetectable by mass spectrometry in the quantities used for our experiment. As we placed our screen's emphasis on minimal false-positives, *i.e.*, low number of falsely reported interaction partners, rather than minimal a few false-negatives, *i.e.*, identification of all known partners, absence of the Argonaute proteins does not diminish the quality of our results. A list of proteins reported to interact with DDX6, but not observed in this study, is provided in the Supplementary Material.

Recent studies identified a physical protein interaction network associated with miRNA biogenesis and regulation, using a proteomic approach [46,53]. The authors listed DDX6-interacting proteins, including NUFIP2, FAM195A and FAM195B, but without further validation. As very little is known about the three proteins, we confirm the interaction and we characterized the function of these proteins with respect to RNA-protein complex interactions. GRAN1 and GRAN2 bind DDX6 and are localized to the cytoplasm under normal conditions. Upon stress, GRAN1 and GRAN2 re-localize to stress granules, suggesting a potential role in translation repression in response to stress and presenting new stress granule components. This dynamic localization to stress granules may be facilitated by the Q/N-rich region in GRAN1. Due to their aggregation-prone nature, Q/N rich regions can be sufficient for localization of a variety of human proteins to P bodies [59,60]. As stress granule proteins also tend to have Q/N rich regions (e.g., ATXN2), the sequence may serve a re-localization function as well. Because GRAN1 and GRAN2 also interact with each other, GRAN2 could be recruited to stress granules via its interaction with GRAN1. In contrast to other interaction partners also reported in yeast, GRAN1 and GRAN2 have orthologs in other vertebrates, but not invertebrates or unicellular eukaryotes—suggesting that their role with DDX6 evolved only recently.

The stress granule protein NUFIP2 is another novel DDX6 interaction partner which we characterized further. NUFIP2 was originally identified through its interaction with the Fragile X mental retardation protein FMR1, but nothing else is known about the protein. Interestingly, FMR1 and its homolog FXR2 were also identified as interacting with DDX6 in this screen, suggesting a role of FMR1/FXR2 in stress that has not been described before. However, given the low relative quantification of each of these proteins in our experiments, the interaction between DDX6 and FMR1/FXR2 may be transient or indirect and mediated by the much more abundant NUFIP2. Both DDX6 and the FMR proteins are noted for their roles in translation repression, and in Drosophila, these proteins have been found to co-localize in neuronal granules, suggesting that they can work in the same pathway [93]. The common interaction with NUFIP2 suggests that further study of this protein may shed light on the nature of translation repression in stress granules. As a side note,

NUFIP2 also contains a Q/N rich region (as well as a proline-rich region), which might explain its localization to stress granules.

Studies of protein-protein interactions can often identify potential new functions for a protein through analysis of the known functions of its interaction partners. Table 1 and Figure 5A,B show several proteins which function in RNA splicing. DDX6 has not previously been associated with splicing, and these data suggest a novel role for DDX6 that may explain its presence in the nucleus. Supporting this hypothesis, several mass spectrometry studies in yeast and human have identified DDX6 as a potential component of the spliceosome [94–96]. This observation could be explained by the fact that many nuclear mRNP that co-localize in P-bodies and stress granules during stress include factors involved in transcription, 3' end processing, splicing and export, which might affect also nuclear events [97].

Finally, we also detected an interaction between DDX6 and the E3 SUMO ligase TIF1β. All evidence established to date says that TIF1β is an exclusively nuclear protein [98]. However, while DDX6 is primarily cytoplasmic, there is evidence that it shuttles between the nucleus and cytoplasm, creating an opportunity for sumoylation by TIF1β [99]. We confirmed that DDX6 is indeed sumoylated (Figure 5C) [70], and also demonstrate significant SUMOylation for the DDX6 interactome (Figure 5D). One intriguing hypothesis for the mechanism of SUMOylation amongst these RNA-binding proteins is based on the fact that SUMO is one of the most soluble of all known proteins [100], and it may be involved in preventing aggregation within densely packed cellular structures such as these granules [101]. As many or most of the DDX6-interacting proteins localize to P bodies and/or stress granules, and this localization is known to depend on a variety of aggregation-prone domains, we hypothesize that maintenance of a certain level of sumoylation of these proteins prevents uncontrolled aggregation during the assembly of cytoplasmic mRNP granules. Uncontrolled mRNP assembly via these low complexity domains has been posited to contribute to a variety of neurodegenerative disorders [102].

4. Experimental Section

4.1. Generation of Cell Lines

pENTR constructs were generated by PCR amplification of the respective coding sequences (CDS) from Flp-In 293 T-REx derived cDNA, followed by restriction digest and ligation into pENTR4 backbone (Invitrogen, Carlsbad, CA, USA). pENTR vectors carrying CDS were recombined into pFRT/TO/FLAG/HA-DEST destination vector using GATEWAY LR recombinase according to manufacturer's protocol (Life Technologies, Carlsbad, CA, USA). Cell lines stably expressing FLAG/HA-tagged DDX6 protein were generated by co-transfection of pFRT/TO/FLAG/HA constructs with pOG44 into Flp-In 293 T-REx cells (Life Technologies). Cells were selected by exchanging zeocin for 100 μg/mL hygromycin, and monoclonal colonies were isolated.

4.2. Cell Culture

HEK-293 cells (ATCC) and derivatives were cultured in a 37 °C incubator with 5% CO_2, in DMEM (Sigma, St Louis, MO, USA) supplemented with 10% FBS (Atlanta Biologicals, Norcross, GA, USA)

and 1% penicillin-streptomycin-Fungizone (Life Technologies). For arsenite treatment, cells were incubated with 50 mM sodium (meta)arsenite ($NaAsO_2$, Sigma) for 1 h. For DDX6-FLAG-HA induction, cells were treated with 1 μg/mL doxycycline (Sigma) for 18 h.

4.3. Immunoprecipitation

For each sample, one 15 cm plate of cells at 80% confluency was rinsed with cold PBS, scraped into 2 mL NP-40 buffer (50 mM HEPES pH 7.5, 150 mM KCl, 2 mM EDTA, 1% NP40, one Complete mini protease inhibitor tablet and one PhosStop tablet per 10 mL (Roche, Basel, Switzerland)) and incubated on ice for 20 min. Protein lysates were then spun at 14,000 RPM for 10 min at 4 °C, and supernatant was used as the protein sample. The lysates were first incubated for 1 h at 4 °C with anti-FLAG agarose beads (Sigma) for the tandem immunoprecipitation, or with Protein G Dynabeads (Life Technologies) bound to an antibody recognizing GRAN2 (Sigma, HPA045542). The beads were washed 3 times in wash buffer (50 mM HEPES pH 7.5, 150 mM KCl, 2 mM EDTA, 0.5% NP40). At this point, some samples were incubated for 10 min at room temperature with 250 units benzonase (Sigma). For the tandem immunoprecipitation, protein complexes were eluted from the beads by 2 incubations with 3XFLAG peptide (Sigma, 100 μg/mL) for 5 min each. The resulting eluate was incubated with Protein G Dynabeads bound to an anti-HA antibody (Sigma, H3663) for 45 min at 4 °C. The bead-bound proteins were then washed 3 times with wash buffer, and either boiled in Laemmli buffer for Western blot (Biorad, Hercules, CA, USA), or washed 3 more times in 25 mM ammonium bicarbonate (ABC) for preparation for mass spectrometry analysis.

4.4. Western Blot

Lysates were prepared as for immunoprecipitation, using RIPA buffer (50 mM Tris pH 7.5, 1% NP40, 0.1% SDS, 0.5% sodium deoxycholate, 150 mM NaCl, one Complete mini protease inhibitor tablet and 1 PhosStop tablet per 10 mL) in place of NP-40 buffer. Equal protein amounts were run on SDS-PAGE gels, transferred via wet electroblotting, and blocked in 5% milk in TBS-T (50 mM Tris pH 7.5, 150 mM NaCl, 0.1% Tween-20). The following primary antibodies were incubated with the blots overnight at a dilution of 1:1000 unless otherwise noted: anti-DDX6 (Abcam, Cambridge, United Kingdom, 4967), anti-FLAG (Sigma, F3165), anti-beta-actin (Cell Signaling, Beverly, MA, USA, 4967), anti-HA (Sigma, H6908), anti-NUFIP2 (Sigma, HPA017344, 1:250), anti-GRAN2 (Sigma, HPA045542, 1:250), anti-GRAN1 (ProteinTech, Chicago, IL, USA, 20808-1-AP), anti-SUMO1 (Abcam, ab32058). HRP-conjugated secondary antibodies were used at a dilution of 1:5000 for 1 h (GE Healthcare, Little Chalfont, UK).

4.5. Blue Native Polyacrylamide Gel Electrophoresis

A single anti-FLAG immunoprecipitation step was performed as described above, including elution with the 3X FLAG peptide. Eluates were separated using the NativePAGE system (Life Technologies) according to the manufacturer's instructions, on a 1 mm 3%−12% Bis-Tris gel. Gel bands from the entire lane were cut with a width of 2 mM from a GelCode Blue-stained gel (Pierce Biotechnology, Waltham, MA, USA), and processed for analysis by mass spectrometry as described below.

4.6. Sample Preparation for Mass Spectrometry

For immunoprecipitation-derived samples, bead-bound proteins from immunoprecipitation experiments were digested and eluted by direct incubation with 50 ng trypsin in ABC overnight at 37 °C. The eluate was then reduced with dithiothreitol (DTT) and then alkylated with iodoacetamide (IAA). Formic acid and acetonitrile were added to final concentrations of 0.1% and 5% respectively. For gel slices, samples were destained in a buffer containing acetonitrile and ABC, reduced with DTT and then alkylated with IAA. The gel slices were dehydrated with acetonitrile, then resuspended with a trypsin digestion solution (100 ng trypsin per sample). Samples were digested overnight at 37 °C. All samples were cleaned with Aspire desalting tips (Thermo Fisher Scientific, New York, NY, USA) according to the manufacturer's instructions as the final step before mass spectrometry analysis.

4.7. Mass Spectrometry

Mass spectrometry analysis was performed on an LTQ Orbitrap (Thermo Scientific) coupled to an Eksigent nano-LC Ultra HPLC (Absciex, Framingham, MA, USA). Samples were run on a 180 min (entire immunoprecipitation samples) or 30 min (gel slices) nonlinear gradient from 2% to 41% acetonitrile in 0.1% formic acid. Survey full-scan mass spectra were acquired from 300–2000 *m/z*, with a resolution of 60,000. The top 20 most intense ions from the survey scan were isolated and fragmented in the linear ion trap by collision-induced dissociation (normalized collision energy = 35 eV). The dynamic exclusion list (n = 500) used a retention time of 90 s and a repeat duration of 45 s (repeat count = 1), and preview scan mode was enabled. Ions of charge state = 1 or unassigned charge states were rejected.

4.8. Immunofluorescence Imaging

Cells were grown on fibronectin-coated coverslips (BD Biosciences), and fixed for 15 min in 4% paraformaldehyde followed by 10 min in cold methanol [90]. Primary antibodies were incubated for 1 h or overnight at the following concentrations: DDX6 (Santa Cruz Biotechnology, Dallas, TX, USA, sc-376433, 1:25), DCP1a (Abcam, ab47811), HA (Roche, 11867423001), NUFIP2 (Sigma, HPA017344, 1:250), GRAN1 (ProteinTech, 20808-1-AP, 1:250), GRAN2 (Sigma, HPA045542, 1:500), PABPC1 (Abcam, ab6125, 1:1000). Fluorescence-conjugated secondary antibodies were incubated for 1 h at a 1:1000 dilution (Molecular Probes, Waltham, MA, USA).

4.9. Bioinformatics and Data Analysis

Evidence for previously established protein-protein interactions was taken from the BioGRID and INTACT databases [55,103], and searches of the literature. Functional enrichment of gene lists by GO annotation was performed using the ProfCom_GO statistical framework [104]. Western blots were quantified via the ImageJ program using standard densitometry techniques [105].

4.10. Mass Spectrometry Data Analysis

RAW files from the mass spectrometer were converted to the mzXML format with ReadW (version 4.3.1, which is available in the TransProteomic Pipeline (TPP) platform (http://tools.proteomecenter-.org/software.php)) and then searched against a human proteome database (ENSEMBL 67) with X!Tandem/the Global Proteome Machine Cyclone XE (version 2.2.1 Beavis Informatics Ltd., Winnipeg, Canada) [106]. Searches were conducted using the following parameters: fragment monoisotopic mass error 0.4 Da, parent monoisotopic mass error plus −/+20 ppm, spectrum conditioning dynamic range 100 and total peaks 50, maximum parent charge 4, minimum parent M + H 500.0, minimum fragment *mz* 150.0, minimum peaks 15, cleavage site [RK] [107], maximum missed cleavage sites = 1 with a refinement step for unanticipated cleavage, complete carbamidomethylation of cysteines (+57 Da), partial oxidation of methionine (+16 Da), and partial deamidation of asparagine and glutamine (−1 Da) in the refinement step only. Protein abundance factor (PAF) was calculated as previously described [108], using an average of the three benzonase-treated replicates. The MS/MS data were also searched against a uniprot-based human protein sequence database including protein sequences of common contaminants by MaxQuant version 1.3.0.3. A FASTA file of the human reference proteome was obtained from UniProt (06-2012, 20,231 entries) [107]. For the searches, trypsin was defined as the protease. The search included carbamidomethyl of cysteine as a fixed modification and N-acetylation of protein and oxidation of methionine as variable modifications. Up to two missed cleavages were allowed for protease digestion and peptide had to be fully tryptic. The mass spectrometry proteomics data have been deposited to the ProteomeXchange Consortium via the PRIDE partner repository [109] with the data identifier PXD002070.

4.11. Sumoylation Bioinformatics Analysis

The software SUMOsp was used to identify sumoylation sites, with the “high-confidence” cutoff values [110]. Statistical significance of enrichment of both sumoylated proteins and sumoylation sites was calculated using hypergeometric distributions.

5. Conclusions

In sum, its multitude of interaction partners and memberships in protein complexes places DDX6 into a key position with a central role in RNA localization and metabolism. While several of the interaction partners have been known before, no study has placed DDX6 into the center of its interaction network, screening for interaction partners both in a comprehensive and highly specific way, minimizing the false-positive rates that are normally high. We present the first study, generate new hypotheses on the protein SUMOylation in DDX6 function and its putative role in splicing, and describe new stress granule components.

Acknowledgements

Christine Vogel acknowledges funding by the NIH (Ro1 GM113237), the DOD (Hypothesis Testing Award PC121532), NYU Whitehead Foundation, the NYU University Research Challenge Fund, and the Zegar Family Foundation Fund for Genomics Research at New York University.

Author Contributions

Rebecca Bish and Christine Vogel conceived the project. Rebecca Bish, Zhe Cheng, Dolores Hambardzumyan, Mathias Munschauer, and Markus Landthaler conducted the experiments. Rebecca Bish, Nerea Cuevas-Polo, and Christine Vogel analyzed the data and wrote the manuscript.

Conflicts of Interest

The authors declare no conflict of interest.

References

1. De Sousa Abreu, R.; Penalva, L.O.; Marcotte, E.M.; Vogel, C. Global signatures of protein and mRNA expression levels. *Mol. Biosyst.* **2009**, *5*, 1512–1526.
2. Maier, T.; Guell, M.; Serrano, L. Correlation of mRNA and protein in complex biological samples. *FEBS Lett.* **2009**, *583*, 3966–3973.
3. Schwanhausser, B.; Busse, D.; Li, N.; Dittmar, G.; Schuchhardt, J.; Wolf, J.; Chen, W.; Selbach, M. Global quantification of mammalian gene expression control. *Nature* **2011**, *473*, 337–342.
4. Vogel, C.; Marcotte, E.M. Insights into the regulation of protein abundance from proteomic and transcriptomic analyses. *Nat. Rev. Genet.* **2012**, *13*, 227–232.
5. Baltz, A.G.; Munschauer, M.; Schwanhausser, B.; Vasile, A.; Murakawa, Y.; Schueler, M.; Youngs, N.; Penfold-Brown, D.; Drew, K.; Milek, M.; *et al.* The mRNA-bound proteome and its global occupancy profile on protein-coding transcripts. *Mol. Cell.* **2012**, *46*, 674–690.
6. Castello, A.; Fischer, B.; Eichelbaum, K.; Horos, R.; Beckmann, B.M.; Strein, C.; Davey, N.E.; Humphreys, D.T.; Preiss, T.; Steinmetz, L.M.; *et al.* Insights into RNA biology from an atlas of mammalian mRNA-binding proteins. *Cell* **2012**, *149*, 1393–1406.
7. Kwon, S.C.; Yi, H.; Eichelbaum, K.; Fohr, S.; Fischer, B.; You, K.T.; Castello, A.; Krijgsveld, J.; Hentze, M.W.; Kim, V.N. The RNA-binding protein repertoire of embryonic stem cells. *Nat. Struct. Mol. Biol.* **2013**, *20*, 1122–1130.
8. Ostareck, D.H.; Naarmann-de Vries, I.S.; Ostareck-Lederer, A. DDX6 and its orthologs as modulators of cellular and viral RNA expression. *Wiley Interdiscip. Rev. RNA* **2014**, *5*, 659–678.
9. Iio, A.; Takagi, T.; Miki, K.; Naoe, T.; Nakayama, A.; Akao, Y. DDX6 post-transcriptionally down-regulates miR-143/145 expression through host gene NCR143/145 in cancer cells. *Biochim. Biophys. Acta* **2013**, *1829*, 1102–1110.
10. Akao, Y.; Matsumoto, K.; Ohguchi, K.; Nakagawa, Y.; Yoshida, H. Human DEAD-box/RNA unwindase Rck/p54 contributes to maintenance of cell growth by affecting cell cycle in cultured cells. *Int. J. Oncol.* **2006**, *29*, 41–48.
11. Perez-Vilaro, G.; Fernandez-Carrillo, C.; Mensa, L.; Miquel, R.; Sanjuan, X.; Forns, X.; Pérez-del-Pulgar, S.; Díez, J. Hepatitis C virus infection inhibits P-body granule formation in human livers. *J. Hepatol.* **2015**, *62*, 785–790.

12. Scheller, N.; Mina, L.B.; Galao, R.P.; Chari, A.; Gimenez-Barcons, M.; Noueiry, A.; Fischer, U.; Meyerhans, A.; Díez, J. Translation and replication of hepatitis C virus genomic RNA depends on ancient cellular proteins that control mRNA fates. *Proc. Natl. Acad. Sci. USA* **2009**, *106*, 13517–13522.
13. Pimentel, J.; Boccaccio, G.L. Translation and silencing in RNA granules: A tale of sand grains. *Front. Mol. Neurosci.* **2014**, doi:10.3389/fnmol.2014.00068.
14. Coller, J.M.; Tucker, M.; Sheth, U.; Valencia-Sanchez, M.A.; Parker, R. The DEAD box helicase, Dhh1p, functions in mRNA decapping and interacts with both the decapping and deadenylase complexes. *RNA* **2001**, *7*, 1717–1727.
15. Fischer, N.; Weis, K. The DEAD box protein Dhh1 stimulates the decapping enzyme Dcp1. *EMBO J*. **2002**, *21*, 2788–2797.
16. Coller, J.; Parker, R. General translational repression by activators of mRNA decapping. *Cell* **2005**, *122*, 875–886.
17. Sweet, T.; Kovalak, C.; Coller, J. The DEAD-box protein Dhh1 promotes decapping by slowing ribosome movement. *PLoS Biol.* **2012**, *10*, e1001342.
18. Nissan, T.; Rajyaguru, P.; She, M.; Song, H.; Parker, R. Decapping activators in Saccharomyces cerevisiae act by multiple mechanisms. *Mol. Cell* **2010**, *39*, 773–783.
19. Su, H.; Meng, S.; Lu, Y.; Trombly, M.I.; Chen, J.; Lin, C.; Turk, A.; Wang, X. Mammalian hyperplastic discs homolog EDD regulates miRNA-mediated gene silencing. *Mol. Cell.* **2011**, *43*, 97–109.
20. Rouya, C.; Siddiqui, N.; Morita, M.; Duchaine, T.F.; Fabian, M.R.; Sonenberg, N. Human DDX6 effects miRNA-mediated gene silencing via direct binding to CNOT1. *RNA* **2014**, *20*, 1398–1409.
21. Akao, Y.; Seto, M.; Yamamoto, K.; Iida, S.; Nakazawa, S.; Inazawa, J.; Abe, T.; Takahashi, T.; Ueda, R. The RCK gene associated with t(11;14) translocation is distinct from the MLL/ALL-1 gene with t(4;11) and t(11;19) translocations. *Cancer Res*. **1992**, *52*, 6083–6087.
22. Lin, F.; Wang, R.; Shen, J.J.; Wang, X.; Gao, P.; Dong, K.; Zhang, H.Z. Knockdown of RCK/p54 expression by RNAi inhibits proliferation of human colorectal cancer cells *in vitro* and *in vivo*. *Cancer Biol. Ther.* **2008**, *7*, 1669–1676.
23. Nakagawa, Y.; Morikawa, H.; Hirata, I.; Shiozaki, M.; Matsumoto, A.; Maemura, K.; Nishikawa, T.; Niki, M.; Tanigawa, N.; Ikegami, M.; *et al*. Overexpression of Rck/p54, a DEAD box protein, in human colorectal tumours. *Br. J. Cancer* **1999**, *80*, 914–917.
24. Stary, S.; Vinatzer, U.; Mullauer, L.; Raderer, M.; Birner, P.; Streubel, B. t(11;14)(q23;q32) involving IGH and DDX6 in nodal marginal zone lymphoma. *Genes Chromosomes Cancer* **2013**, *52*, 33–43.
25. Chahar, H.S.; Chen, S.; Manjunath, N. P-body components LSM1, GW182, DDX3, DDX6 and XRN1 are recruited to WNV replication sites and positively regulate viral replication. *Virology* **2013**, *436*, 1–7.
26. Jangra, R.K.; Yi, M.; Lemon, S.M. DDX6 (Rck/p54) is required for efficient hepatitis C virus replication but not for internal ribosome entry site-directed translation. *J. Virol.* **2010**, *84*, 6810–6824.

27. Reed, J.C.; Molter, B.; Geary, C.D.; McNevin, J.; McElrath, J.; Giri, S.; Klein, K.C.; Lingappa, J.R. HIV-1 Gag co-opts a cellular complex containing DDX6, a helicase that facilitates capsid assembly. *J. Cell. Biol.* **2012**, *198*, 439–456.
28. Yu, S.F.; Lujan, P.; Jackson, D.L.; Emerman, M.; Linial, M.L. The DEAD-box RNA helicase DDX6 is required for efficient encapsidation of a retroviral genome. *PLoS Pathog.* **2011**, *7*, e1002303.
29. Strahl-Bolsinger, S.; Tanner, W. A yeast gene encoding a putative RNA helicase of the "DEAD"-box family. *Yeast* **1993**, *9*, 429–432.
30. Maekawa, H.; Nakagawa, T.; Uno, Y.; Kitamura, K.; Shimoda, C. The $Ste13^{+}$ gene encoding a putative RNA helicase is essential for nitrogen starvation-induced G1 arrest and initiation of sexual development in the fission yeast *Schizosaccharomyces pombe*. *Mol. Gen. Gene* **1994**, *244*, 456–464.
31. Navarro, R.E.; Shim, E.Y.; Kohara, Y.; Singson, A.; Blackwell, T.K. Cgh-1, a conserved predicted RNA helicase required for gametogenesis and protection from physiological germline apoptosis in *C. elegans*. *Development* **2001**, *128*, 3221–3232.
32. De Valoir, T.; Tucker, M.A.; Belikoff, E.J.; Camp, L.A.; Bolduc, C.; Beckingham, K. A second maternally expressed Drosophila gene encodes a putative RNA helicase of the "DEAD box" family. *Proc. Natl. Acad. Sci. USA* **1991**, *88*, 2113–2117.
33. Ladomery, M.; Wade, E.; Sommerville, J. Xp54, the Xenopus homologue of human RNA helicase p54, is an integral component of stored mRNP particles in oocytes. *Nucleic Acids Res*. **1997**, *25*, 965–973.
34. Lu, D.; Yunis, J.J. Cloning, expression and localization of an RNA helicase gene from a human lymphoid cell line with chromosomal breakpoint 11q23.3. *Nucleic Acids Res.* **1992**, *20*, 1967–1972.
35. Cougot, N.; Babajko, S.; Seraphin, B. Cytoplasmic foci are sites of mRNA decay in human cells. *J. Cell. Biol.* **2004**, *165*, 31–40.
36. Moser, J.J.; Fritzler, M.J. Relationship of other cytoplasmic ribonucleoprotein bodies (cRNPB) to GW/P bodies. *Adv. Exp. Med. Biol.* **2013**, *768*, 213–242.
37. Nonhoff, U.; Ralser, M.; Welzel, F.; Piccini, I.; Balzereit, D.; Yaspo, M.L.; Lehrach, H.; Krobitsch, S. Ataxin-2 interacts with the DEAD/H-box RNA helicase DDX6 and interferes with P-bodies and stress granules. *Mol. Biol. Cell.* **2007**, *18*, 1385–1396.
38. Wilczynska, A.; Aigueperse, C.; Kress, M.; Dautry, F.; Weil, D. The translational regulator CPEB1 provides a link between dcp1 bodies and stress granules. *J. Cell. Sci.* **2005**, *118*, 981–992.
39. Presnyak, V.; Coller, J. The DHH1/RCKp54 family of helicases: An ancient family of proteins that promote translational silencing. *Biochim. Biophys. Acta.* **2013**, *1829*, 817–823.
40. Fenger-Gron, M.; Fillman, C.; Norrild, B.; Lykke-Andersen, J. Multiple processing body factors and the ARE binding protein TTP activate mRNA decapping. *Mol. Cell.* **2005**, *20*, 905–915.
41. De Vries, S.; Naarmann-de Vries, I.S.; Urlaub, H.; Lue, H.; Bernhagen, J.; Ostareck, D.H.; Ostareck-Lederer, A. Identification of DEAD-box RNA helicase 6 (DDX6) as a cellular modulator of vascular endothelial growth factor expression under hypoxia. *J. Biol. Chem.* **2013**, *288*, 5815–5827.

42. Minshall, N.; Thom, G.; Standart, N. A conserved role of a DEAD box helicase in mRNA masking. *RNA* **2001**, *7*, 1728–1742.
43. Stoecklin, G.; Kedersha, N. Relationship of GW/P-bodies with stress granules. *Adv. Exp. Med. Biol.* **2013**, *768*, 197–211.
44. Chu, C.Y.; Rana, T.M. Translation repression in human cells by microRNA-induced gene silencing requires RCK/p54. *PLoS Biol*. **2006**, *4*, e210.
45. Nishihara, T.; Zekri, L.; Braun, J.E.; Izaurralde, E. miRISC recruits decapping factors to miRNA targets to enhance their degradation. *Nucleic Acids Res.* **2013**, *41*, 8692–8705.
46. Nicklas, S.; Okawa, S.; Hillje, A.L.; Gonzalez-Cano, L.; del Sol, A.; Schwamborn, J.C. The RNA helicase DDX6 regulates cell-fate specification in neural stem cells via miRNAs. *Nucleic Acids Res*. **2015**, *43*, 2638–2654.
47. Chen, Y.; Boland, A.; Kuzuoglu-Ozturk, D.; Bawankar, P.; Loh, B.; Chang, C.T.; Weichenrieder, O.; Izaurralde, E. A DDX6-CNOT1 complex and W-binding pockets in CNOT9 reveal direct links between miRNA target recognition and silencing. *Mol. Cell* **2014**, *54*, 737–750.
48. Ozgur, S.; Chekulaeva, M.; Stoecklin, G. Human Pat1b connects deadenylation with mRNA decapping and controls the assembly of processing bodies. *Mol. Cell. Biol*. **2010**, *30*, 4308–4323.
49. Kaehler, C.; Isensee, J.; Nonhoff, U.; Terrey, M.; Hucho, T.; Lehrach, H.; Krobitsch, S. Ataxin-2-like is a regulator of stress granules and processing bodies. *PLoS ONE* **2012**, *7*, e50134.
50. Parker, R.; Sheth, U. P bodies and the control of mRNA translation and degradation. *Mol. Cell* **2007**, *25*, 635–646.
51. Phalora, P.K.; Sherer, N.M.; Wolinsky, S.M.; Swanson, C.M.; Malim, M.H. HIV-1 replication and APOBEC3 antiviral activity are not regulated by P bodies. *J. Virol.* **2012**, *86*, 11712–11724.
52. Andrei, M.A.; Ingelfinger, D.; Heintzmann, R.; Achsel, T.; Rivera-Pomar, R.; Lührmann, R. A role for eIF4E and eIF4E-transporter in targeting mRNPs to mammalian processing bodies. *RNA* **2005**, *11*, 717–727.
53. Chatr-Aryamontri, A.; Breitkreutz, B.J.; Oughtred, R.; Boucher, L.; Heinicke, S.; Chen, D.; Stark, C.; Breitkreutz, A.; Kolas, N.; O'Donnell, L.; *et al.* The BioGRID interaction database: 2015 update. *Nucleic Acids Res.* **2015**, *43*, D470–D478.
54. Li, S.; Wang, L.; Fu, B.; Berman, M.A.; Diallo, A.; Dorf, M.E. TRIM65 regulates microRNA activity by ubiquitination of TNRC6. *Proc. Natl. Acad. Sci. USA* **2014**, *111*, 6970–6975.
55. Rolland, T.; Tasan, M.; Charloteaux, B.; Pevzner, S.J.; Zhong, Q.; Sahni, N.; Yi, S.; Lemmens, I.; Fontanillo, C.; Mosca, R.; *et al.* A proteome-scale map of the human interactome network. *Cell* **2014**, *159*, 1212–1226.
56. Bardoni, B.; Castets, M.; Huot, M.E.; Schenck, A.; Adinolfi, S.; Corbin, F.; Pastore, A.; Khandjian, E.W.; Mandel, J.L. 82-FIP, a novel FMRP (fragile X mental retardation protein) interacting protein, shows a cell cycle-dependent intracellular localization. *Hum. Mol. Genet.* **2003**, *12*, 1689–1698.
57. Ramos, A.; Hollingworth, D.; Adinolfi, S.; Castets, M.; Kelly, G.; Frenkiel, T.A.; Bardoni, B.; Pastore, A. The structure of the N-terminal domain of the fragile X mental retardation protein: A platform for protein-protein interaction. *Structure* **2006**, *14*, 21–31.
58. Hornbeck, P.V.; Kornhauser, J.M.; Tkachev, S.; Zhang, B.; Skrzypek, E.; Murray, B.; Latham, V.; Sullivan, M. PhosphoSitePlus: A comprehensive resource for investigating the structure and

function of experimentally determined post-translational modifications in man and mouse. *Nucleic Acids Res.* **2012**, *40*, D261–D270.

59. Punta, M.; Coggill, P.C.; Eberhardt, R.; Mistry, J.; Tate, J.; Hotz, H.; Ceric, G.; Forslund, K.; Eddy, S.R.; Sonnhammer, E.L.L.; *et al.* The Pfam protein families database. *Nucleic Acids Res*. **2012**, *40*, D290–D301.
60. Bogerd, H.P.; Fridell, R.A.; Benson, R.E.; Hua, J.; Cullen, B.R. Protein sequence requirements for function of the human T-cell leukemia virus type 1 Rex nuclear export signal delineated by a novel *in vivo* randomization-selection assay. *Mol. Cell. Biol.* **1996**, 16, 4207–4214.
61. La Cour, T.; Kiemer, L.; Molgaard, A.; Gupta, R.; Skriver, K.; Brunak, S. Analysis and prediction of leucine-rich nuclear export signals. *Protein Eng. Des. Sel.* **2004**, *17*, 527–536.
62. Reijns, M.A.; Alexander, R.D.; Spiller, M.P.; Beggs, J.D. A role for Q/N-rich aggregation-prone regions in P-body localization. *J. Cell. Sci.* **2008**, *121*, 2463–2472.
63. Kato, M.; Han, T.W.; Xie, S.; Shi, K.; Du, X.; Wu, L.C.; Mirzaei, H.; Goldsmith, E.J.; Longgood, J.; Pei, J.; *et al*. Cell-free formation of RNA granules: Low complexity sequence domains form dynamic fibers within hydrogels. *Cell* **2012**, *149*, 753–767.
64. Schagger, H.; Cramer, W.A.; von Jagow, G. Analysis of molecular masses and oligomeric states of protein complexes by blue native electrophoresis and isolation of membrane protein complexes by two-dimensional native electrophoresis. *Anal. Biochem.* **1994**, *217*, 220–230.
65. Schagger, H.; von Jagow, G. Blue native electrophoresis for isolation of membrane protein complexes in enzymatically active form. *Anal. Biochem.* **1991**, *199*, 223–231.
66. Wittig, I.; Braun, H.P.; Schagger, H. Blue native PAGE. *Nat. Protoc.* **2006**, *1*, 418–428.
67. Petersen-Mahrt, S.K.; Estmer, C.; Ohrmalm, C.; Matthews, D.A.; Russell, W.C.; Russell, W.C.; Akusjärvi, G. The splicing factor-associated protein, p32, regulates RNA splicing by inhibiting ASF/SF2 RNA binding and phosphorylation. *EMBO J*. **1999**, *18*, 1014–1024.
68. Ivanov, A.V.; Peng, H.; Yurchenko, V.; Yap, K.L.; Negorev, D.G.; Schultz, D.C.; Psulkowski, E.; Fredericks, W.J.; White, D.E.; Maul, G.G.; *et al.* PHD domain-mediated E3 ligase activity directs intramolecular sumoylation of an adjacent bromodomain required for gene silencing. *Mol. Cell* **2007**, *28*, 823–837.
69. Liang, Q.; Deng, H.; Li, X.; Wu, X.; Tang, Q.; Chang, T.H.; Peng, H.; Rauscher, F.J., 3rd; Ozato, K.; Zhu, F. Tripartite motif-containing protein 28 is a small ubiquitin-related modifier E3 ligase and negative regulator of IFN regulatory factor 7. *J. Immunol.* **2011**, *187*, 4754–4763.
70. Grant, M.M. Identification of SUMOylated proteins in neuroblastoma cells after treatment with hydrogen peroxide or ascorbate. *BMB Rep.* **2010**, *43*, 720–725.
71. Blomster, H.A.; Hietakangas, V.; Wu, J.; Kouvonen, P.; Hautaniemi, S.; Sistonen, L. Novel proteomics strategy brings insight into the prevalence of SUMO-2 target sites. *Mol. Cell. Proteomics* **2009**, *8*, 1382–1390.
72. Golebiowski, F.; Matic, I.; Tatham, M.H.; Cole, C.; Yin, Y.; Nakamura, A.; Cox, J.; Barton, G.J.; Mann, M.; Hay, R.T. System-wide changes to SUMO modifications in response to heat shock. *Sci. Signal.* **2009**, doi:10.1126/scisignal.2000282.

73. Lamoliatte, F.; Bonneil, E.; Durette, C.; Caron-Lizotte, O.; Wildemann, D.; Zerweck, J.; Wenshuk, H.; Thibault, P. Targeted identification of SUMOylation sites in human proteins using affinity enrichment and paralog-specific reporter ions. *Mol. Cell. Proteomics* **2013**, *12*, 2536–2550.
74. Manza, L.L.; Codreanu, S.G.; Stamer, S.L.; Smith, D.L.; Wells, K.S.; Roberts, R.L.; Liebler, D.C. Global shifts in protein sumoylation in response to electrophile and oxidative stress. *Chem. Res. Toxicol.* **2004**, *17*, 1706–1715.
75. Miller, M.J.; Barrett-Wilt, G.A.; Hua, Z.; Vierstra, R.D. Proteomic analyses identify a diverse array of nuclear processes affected by small ubiquitin-like modifier conjugation in Arabidopsis. *Proc. Natl. Acad. Sci. USA* **2010**, *107*, 16512–16517.
76. Miller, M.J.; Scalf, M.; Rytz, T.C.; Hubler, S.L.; Smith, L.M.; Vierstra, R.D. Quantitative proteomics reveals factors regulating RNA biology as dynamic targets of stress-induced SUMOylation in Arabidopsis. *Mol. Cell. Proteomics* **2013**, *12*, 449–463.
77. Vertegaal, A.C.; Andersen, J.S.; Ogg, S.C.; Hay, R.T.; Mann, M.; Lamond, A.I. Distinct and overlapping sets of SUMO-1 and SUMO-2 target proteins revealed by quantitative proteomics. *Mol. Cell. Proteomics* **2006**, *5*, 2298–2310.
78. Westman, B.J.; Lamond, A.I. A role for SUMOylation in snoRNP biogenesis revealed by quantitative proteomics. *Nucleus* **2011**, *2*, 30–37.
79. Hendriks, I.A.; D'Souza, R.C.; Yang, B.; Verlaan-de Vries, M.; Mann, M.; Vertegaal, A.C. Uncovering global SUMOylation signaling networks in a site-specific manner. *Nat. Struct. Mol. Biol.* **2014**, *21*, 927–936.
80. Blomster, H.A.; Imanishi, S.Y.; Siimes, J.; Kastu, J.; Morrice, N.A.; Eriksson, J.E.; Sistonen, L. *In vivo* identification of sumoylation sites by a signature tag and cysteine-targeted affinity purification. *J. Biol. Chem.* **2010**, *285*, 19324–19329.
81. Bruderer, R.; Tatham, M.H.; Plechanovova, A.; Matic, I.; Garg, A.K.; Hay, R.T. Purification and identification of endogenous polySUMO conjugates. *EMBO Rep*. **2011**, *12*, 142–148.
82. Galisson, F.; Mahrouche, L.; Courcelles, M.; Bonneil, E.; Meloche, S.; Chelbi-Alix, M.K.; Thibaultc, P. A novel proteomics approach to identify SUMOylated proteins and their modification sites in human cells. *Mol. Cell. Proteomics* **2011**, *10*, 65–67.
83. Matic, I.; Schimmel, J.; Hendriks, I.A.; van Santen, M.A.; van de Rijke, F.; van Dam, H.; Gnad, F.; Mann, M.; Vertegaal, A.C. Site-specific identification of SUMO-2 targets in cells reveals an inverted SUMOylation motif and a hydrophobic cluster SUMOylation motif. *Mol. Cell* **2010**, *39*, 641–652.
84. Rosas-Acosta, G.; Russell, W.K.; Deyrieux, A.; Russell, D.H.; Wilson, V.G. A universal strategy for proteomic studies of SUMO and other ubiquitin-like modifiers. *Mol. Cell. Proteomics* **2005**, *4*, 56–72.
85. Schimmel, J.; Larsen, K.M.; Matic, I.; van Hagen, M.; Cox, J.; Mann, M.; Andersen, J.S.; Vertegaal, A.C. The ubiquitin-proteasome system is a key component of the SUMO-2/3 cycle. *Mol. Cell. Proteomics* **2008**, *7*, 2107–2122.
86. Tatham, M.H.; Matic, I.; Mann, M.; Hay, R.T. Comparative proteomic analysis identifies a role for SUMO in protein quality control. *Sci. Signal.* **2011**, *4*, 1913–1920.

87. Vertegaal, A.C.; Ogg, S.C.; Jaffray, E.; Rodriguez, M.S.; Hay, R.T.; Andersen, J.S.; Mann, M.; Lamond, A.I. A proteomic study of SUMO-2 target proteins. *J. Biol. Chem.* **2004**, *279*, 33791–33798.
88. Weston, A.; Sommerville, J. Xp54 and related (DDX6-like) RNA helicases: Roles in messenger RNP assembly, translation regulation and RNA degradation. *Nucleic Acids Res.* **2006**, *34*, 3082–3094.
89. Jonas, S.; Izaurralde, E. The role of disordered protein regions in the assembly of decapping complexes and RNP granules. *Genes Dev*. **2013**, *27*, 2628–2641.
90. Kedersha, N.; Anderson, P. Mammalian stress granules and processing bodies. *Methods Enzymol.* **2007**, *431*, 61–81.
91. Chang, L.C.; Lee, F.J. The RNA helicase Dhh1p cooperates with Rbp1p to promote porin mRNA decay via its non-conserved C-terminal domain. *Nucleic Acids Res.* **2012**, *40*, 1331–1344.
92. Ayache, J.; Benard, M.; Ernoult-Lange, M.; Minshall, N.; Standart, N.; Kress, M.; Weil, D. P-body assembly requires DDX6 repression complexes rather than decay or Ataxin2/2L complexes. *Mol. Biol. Cell* **2015**, doi:10.1091/mbc.E15-03-0136.
93. Monzo, K.; Papoulas, O.; Cantin, G.T.; Wang, Y.; Yates, J.R., 3rd; Sisson, J.C. Fragile X mental retardation protein controls trailer hitch expression and cleavage furrow formation in Drosophila embryos. *Proc. Natl. Acad. Sci. USA* **2006**, *103*, 18160–18165.
94. Neubauer, G.; King, A.; Rappsilber, J.; Calvio, C.; Watson, M.; Sleeman, J.; Lamond, A.; Mann, M. Mass spectrometry and EST-database searching allows characterization of the multi-protein spliceosome complex. *Nat. Genet.* **1998**, *20*, 46–50.
95. Sharma, S.; Kohlstaedt, L.A.; Damianov, A.; Rio, D.C.; Black, D.L. Polypyrimidine tract binding protein controls the transition from exon definition to an intron defined spliceosome. *Nat. Struct. Mol. Biol.* **2008**, *15*, 183–191.
96. Stevens, S.W.; Ryan, D.E.; Ge, H.Y.; Moore, R.E.; Young, M.K.; Lee, T.D.; Abelson, J. Composition and functional characterization of the yeast spliceosomal penta-snRNP. *Mol. Cell* **2002**, *9*, 31–44.
97. Buchan, J.R.; Parker, R. Eukaryotic stress granules: The ins and outs of translation. *Mol. Cell* **2009**, *36*, 932–941.
98. O'Geen, H.; Farnham, P.J. TRIM28: The transcription factor encyclopedia. *Genome Biol.* **2012**, doi:10.1186/gb-2012-13-3.
99. Smillie, D.A.; Sommerville, J. RNA helicase p54 (DDX6) is a shuttling protein involved in nuclear assembly of stored mRNP particles. *J. Cell. Sci.* **2002**, *115*, 395–407.
100. Marblestone, J.G.; Edavettal, S.C.; Lim, Y.; Lim, P.; Zuo, X.; Tauseef, R.B. Comparison of SUMO fusion technology with traditional gene fusion systems: Enhanced expression and solubility with SUMO. *Protein Sci*. **2006**, *15*, 182–189.
101. Krumova, P.; Meulmeester, E.; Garrido, M.; Tirard, M.; Hsiao, H.H.; Bossis, G.; Urlaub, H.; Zweckstetter, M.; Kügler, S.; Melchior, F.; *et al.* Sumoylation inhibits alpha-synuclein aggregation and toxicity. *J. Cell. Biol.* **2011**, *194*, 49–60.
102. Ramaswami, M.; Taylor, J.P.; Parker, R. Altered ribostasis: RNA-protein granules in degenerative disorders. *Cell* **2013**, *154*, 727–736.

103. Orchard, S.; Ammari, M.; Aranda, B.; Breuza, L.; Briganti, L.; Broackes-Carter, F.; Campbell, N.H.; Chavali, G.; Chen, C.; del-Toro, N.; *et al.* The MIntAct project—IntAct as a common curation platform for 11 molecular interaction databases. *Nucleic Acids Res.* **2014**, *42*, D358–D363.
104. Antonov, A.V. BioProfiling.de: Analytical web portal for high-throughput cell biology. *Nucleic Acids Res*. **2011**, *39*, W323–W327.
105. Schneider, C.A.; Rasband, W.S.; Eliceiri, K.W. NIH Image to ImageJ: 25 Years of image analysis. *Nat. Methods* **2012**, *9*, 671–675.
106. Fenyo, D.; Eriksson, J.; Beavis, R. Mass spectrometric protein identification using the global proteome machine. *Methods Mol. Biol.* **2010**, *673*, 189–202.
107. Consortium, U.P. Update on activities at the Universal Protein Resource (UniProt) in 2013. *Nucleic Acids Res.* **2012**, *41*, D190–D195.
108. Powell, D.W.; Weaver, C.M.; Jennings, J.L.; McAfee, K.J.; He, Y.; Weil, P.A.; Link, A.J. Cluster analysis of mass spectrometry data reveals a novel component of SAGA. *Mol. Cell. Biol.* **2004**, *24*, 7249–7259.
109. Vizcaino, J.A.; Cote, R.G.; Csordas, A.; Dianes, J.A.; Fabregat, A.; Foster, J.M.; Griss, J.; Alpi, E.; Birim, M.; Contell, J.; *et al.* The PRoteomics IDEntifications (PRIDE) database and associated tools: Status in 2013. *Nucleic Acids Res*. **2013**, *41*, D1063–D1069.
110. Ren, J.; Gao, X.; Jin, C.; Zhu, M.; Wang, X.; Shaw, A.; Wen, L.; Yao, X.; Yu, X. Systematic study of protein sumoylation: Development of a site-specific predictor of SUMOsp 2.0. *Proteomics* **2009**, *9*, 3409–3412.